NTNU
Norwegian University of
Science and Technology

Frequency-domain Roll Motion Analysis of a Transportation Barge Using Stochastic Linearization of Viscous Roll Damping

Anders Juul Weiby

Marine Technology
Submission date: June 2018
Supervisor: Zhen Gao, IMT

Norwegian University of Science and Technology
Department of Marine Technology

Abstract

This thesis is proposed by DNV GL, and presents a comparative study of frequency-domain and time-domain analysis of the roll motion. The goal is to perform a roll motion analysis of a barge-cargo system considering linearized roll damping with application of the stochastic linearization method.

Transportation of large structures causes fatigue damage on the structure. This is due to horizontal acceleration on deck caused by the damping, mainly due to the roll motion. To reduce the roll motion a bilge keel is found to be the most effective mechanism, it reduces the roll motion very well in both zero- and non-zero forward speed. Viscous damping from Eddy-making and bilge keel is found to be the most dominant damping contributions for the barge.

The equation of motion in both frequency domain and time domain are established, and a linearization of the non-linear damping term for roll motion is estimated. Linearity is a requirement when analyzing a problem in frequency domain. The linear equivalent damping term is established for both regular and irregular waves. The principle of equivalent linearization is used, where the energy loss of the equivalent damping shall be the same as the real energy loss per roll cycle.

The roll motion analysis is performed in HydroD/WADAM, where both regular and irregular waves are considered with 45 and 90 degrees wave heading. The quadratic damping is included as fraction of critical quadratic damping, and linearized by the stochastic linearization method. For the irregular wave case, the response spectrum obtained in the frequency domain analysis is compared with results from the time-domain analysis. The results from the frequency-domain analysis is good, and coincide very well with the results from the time-domain analysis, and creates a good basis for a transportation fatigue analysis.

Preface

This is the master thesis carried out spring 2018, as part of a Master's degree with a specialization in Marine Structures at the Department of Marine Technology, Norwegian University of Science and Technology (NTNU) in Trondheim. The idea behind the project is proposed by DNV GL as a comparison to their own study on the topic. The work is based on the project thesis completed fall 2017.

This thesis is supposed to be within the topic of marine structures, however, it shows many similarities with hydrodynamics and has given me a broader understanding of the field of Marine Technology. The reader is expected to have basic knowledge of basic hydrodynamics and dynamic analysis of offshore structures.

Trondheim, June 11, 2018

Anders Juul Weiby

Sammendrag

Denne masteravhandlingen er foreslått av DNV GL, og inneholder en sammenlikningsstudie av frekvensdomene- og tidsdomeneanalyse av rullebevegelsen. Målet er åutføre en rullebevegelsesanalyse av et lekter-last system med tanke pålinearisert rulledemping ved anvendelse av stokastisk linearisering.

Transport av store strukturer fører til tretthetskader påstrukturen. Dette skyldes horisontal akselerasjon pådekk forårsaket av demping, hovedsakelig pågrunn av rullebevegelsen. For åredusere rullebevegelsen er slingrekjøl som den mest effektive mekanismen, den reduserer rullebevegelsen veldig bra i både ved null hastighet og i fart. Viskøs demping fra Eddy-making og slingrekjøl er funnet åvære de mest dominerende dempingsbidragene til lekteren.

Bevegelsesligningen i både frekvensdomene og tidsdomene er etablert, og en linearisering av den ikke-lineære dempingstiden for rullebevegelse er estimert. Linearitet er et krav når man analyserer et problem i frekvensdomene. Den lineære ekvivalente dempingen er etablert for både regulær og uregelmessig sjø. Prinsippet om ekvivalent linearisering brukes, hvor energitapet av ekvivalent demping skal være det samme som det virkelige energitapet per rullesyklus.

Rollbevegelsesanalysen er utført i HydroD/WADAM, hvor både regulær og uregelmessig sjøvurderes med 45 og 90 graders bølgeretning. Den kvadratiske dempingen er inkludert som fraksjon av kritisk kvadratisk dempning, og linearisert med den stokastiske lineariseringsmetoden. For uregelmessig sjø, blir responsspektret som er utregnet i frekvensdomene analysen, sammenlignet med resultater fra tidsdomene analysen. Resultatene fra frekvensdomene analysen er gode, og sammenfaller godt med resultatene fra tidsdomene analysen, og skaper et godt grunnlag for en utmattings analyse.

Acknowledgments

I would like to thank my supervisor Zhen Gao at the Department of Marine Technology for indispensable weekly guidance in the field of hydrodynamics and stochastic analysis. Furthermore, I would like to thank my co-supervisor Limin Yang from DNVGL for the proposed topic and helpful guidance and feedback during this semester.

Additionally, I would also like to thank Zhiyu Jiang at the Department of Marine Technology with helpful guidance in HydroD/WADAM, and Ingrid Mehn-Andersen for providing the data computed in time-domain.

Last but not least I would like to thank my co-workers Lars Gellein Halvorsen and Ole Kristian Vikenes at office A2.023 for creating a good working environment.

Contents

List of Figures

List of Tables

Nomenclature

∇	Differential operator
$\mathbf{n}$	normal vector
$\mathbf{U}$	Velocity
$\mathbf{V}$	Velocity vector
α	JONSWAP parameter
γ	Ratio between max energy in JONSWAP and PM
∇	Volume displacement
Ω	Fluid domain
ω	Wave frequency
ω_p	Peak frequency
$\overline{GM}$	Transversal metacentric height
$\overline{GM}_T$	Transverse metacentric height
ϕ	Velocity potential
ϕ_0	Incident wave
ϕ_D	Diffraction
ϕ_R	Radiation potential
ρ	Density of water

ρ	Water density
σ	Width of the JONSWAP spectrum
τ	Time variable
ε	Error associated with the linearization
ζa	Wave amplitude
A_{44}	Added moment in roll
$F_{exc}(t)$	Wave excitation load
$F_{rad}(t)$	Radiation load
Hs	Significant wave height
p	Pressure
p_a	Ambient pressure
r_{44}	Radius of gyration of roll
r_{44}	Roll radius of gyration
R_{max}	Most probable largest value
$S(\omega)$	Wave spectrum
t	Time
Tp	Peak-period
Tz	Zero up-crossing period
B	Damping
C	Restoring
$E[\cdot]$	Expected value
Fn	Foude number
I	Moment of inertia
L	Length of the barge

M	Mass
T	Period
U	Speed of the vessel
V	Displaced volume of the barge
$A(\omega)$	Added mass
g	Gravity

Abbreviations

VIV	Vortex Induced Vibrations
HTV	Heavy Transport Vessel
COG	Center Of Gravity
DoF	Degrees of Freedom
TD	Time Domain
FD	Frequency Domain
RAO	Response Amplitude Operator
GUI	Graphical User Interface

Chapter 1

Introduction

1.1 Background

Large offshore structures like jackets are commonly built in Asia, where they have big construction yards and cheap supply of labor. This requires a long transportation voyage when the installation site is on the other side of the planet, e.g. Norway. The transportation of these structures is done by barges towed by tugboats or Heavy Transport Vessels (HTV), where the structures will be subjected to fatigue damage from the following causes; vortex-induced vibrations (VIV) due to wind, water impact on the structure, motion in the vessel transferred to the structure, e.g. hogging and sagging, slamming, vibrations and acceleration on deck. Especially the joints where the structure is attached is vulnerable for this type of motions. However, the main cause of fatigue damage during transportation is inertia loads due to wave-induced motions of the barge.

Todays methods to calculate transportation fatigue are not good enough. The fatigue calculation guidance from the DNV GL Marine Operations standard DNVGL-ST-N001 (DNVGL-ST-N001, 2016) is the newest recommended standard from DNV GL. The problem with this standard is that the guidance for calculating transportation fatigue is not complete. They are commonly based on long-term scatter diagrams for the transportation route. However, the deviation in the sea state may be large due to the variable sea conditions during the voyage. This large deviation could give a much higher actual fatigue than predicted. Hence we must consider the variation of environmental conditions

when calculating the fatigue. Analyses required for this guidance are quite comprehensive resulting in many assumptions made. Thus the calculations can be done in many ways, and depends on which assumptions are made by the designers. This problem is what DNV GL want to solve by creating a new more unified understanding of transportation fatigue guidance in the industry.

Roll is coupled to sway and yaw, but we simplify the problem, and consider the roll motion as uncoupled. If we are going to compute realistic roll motion for a ship with forward speed, it should be included. The roll motion can be large, up to 30-40°, which leads to non-linearities in the damping term. The non-linearities means we need to consider viscous effects to get accurate results, only considering potential damping is not sufficient. To solve the equation of motion in frequency domain, we need to linearize it (Pettersen, 2007). One of the topics where the guidance to transportation fatigue analyses are insufficient is how to deal with non-linear viscous roll damping. This is going to be the main topic of this thesis. The barge-cargo system is illustrated in Figure 1.1.

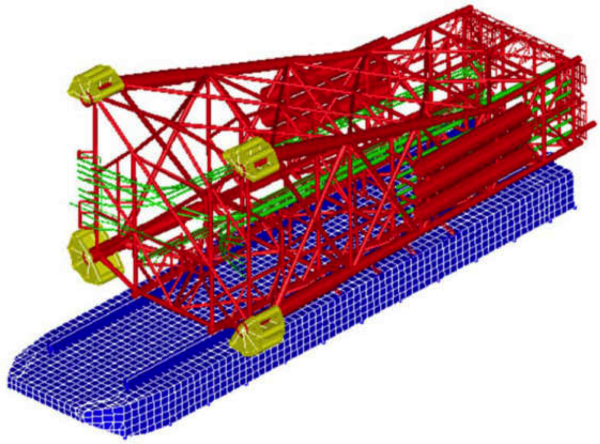

Figure 1.1: Barge-Cargo system

From (Bøe *et al.* , 2017) and (Yang *et al.* , 2018)

1.2 Objective

- Carry out a literature review on sea transportation, wave-induced ship roll motion analysis and in particular on roll damping modeling, frequency-domain hydrodynamic loads and motion analysis, stochastic linearization of quadratic damping.
- Study how to use the software HydroD and WADAM (Wave Analysis by Diffraction and Morison theory). Based on the input data from DNV-GL, establish a frequency-domain hydrodynamic model in HydroD and provide the hydrodynamic results for time-domain modeling in SIMA.
- Perform the basic hydrodynamic analysis and compare the natural periods for heave, roll and pitch with the time-domain results.
- Consider the wave direction of 45 degrees and 90 degrees, regular wave cases with wave amplitude of 1m, use the given quadratic damping and the stochastic linearization methods, perform frequency-domain motion analysis and obtain the roll motion RAO (Response Amplitude Operator). Compare these RAO results with the time-domain results.
- Consider irregular wave cases (Hs=1.5, 2.5, 3.5, 4.5, 5.5, 6.5 m and corresponding Tp=7.5, 8.5, 9.5, 10.5, 11.5, 12.5s), using stochastic linearization methods, obtain roll motion spectra and compare them with the time-domain results.

1.3 Assumptions

To calculate the roll motion response, several assumptions have been made, a list is found below:

- Zero forward speed
- Inviscid and incompressible sea water
- Irrotational fluid motion
- Uncoupled roll motion

1.4 Structure of the report

The report contains 6 chapters structured as follows:

Chapter 1
Introduction of the problem and presentation of the structure of the report.

Chapter 2
Literature review on sea transportation, including sea-fastening where roll damping will be the main focus. There will also be introduced mechanisms to reduce roll motion.

Chapter 3
Description of the theory behind the calculations, which includes wave theory and the equivalent linearization techniques.

Chapter 4
Analysis setup where a brief description of the software will be presented, and a description of the model will be included.

Chapter 5
Results, where the results from the hydrodynamic analysis are presented and discussed. The results from the time-domain analysis are compared with results from the frequency-domain analysis.

Chapter 6
Conclusion and recommendations for further work.

Chapter 2

Literature review

2.1 Transportation procedure

In this chapter, a general description of the transportation method, and issues related to fatigue damage on jackets during transportation on barges will be presented. There will also be focus on the roll damping, and how the damping contributes to fatigue damage.

Towing operations and sea fastening

Towing operations are the most common marine operation. In this particular case, a jacket is transported from Asia to Europe (DNV-RP-H103, 2011). The sea fastening is usually done by welding the cargo to the barge-deck or fasten the cargo by chains (Natskår & Moan, 2010).

The barge is towed by a tugboat. In heavy conditions it will head up against the waves to reduce the roll motion. Extreme values in roll motion will only happen if the tug is failing, or the towing line is breaking. This is why the mean sea state is more relevant for the fatigue damage.

2.1.1 Fatigue damage during transportation

A considerable issue related to transportation of cargo on barges is fatigue damage. In this case, the transportation is concerning large volume structures; hence we are dealing with inertia dominated loads. The inertia loads are due to

the wave-induced motion of the barge and wave induced bending and torsion of the barge.
In addition to wave-induced fatigue damage, we have other contributions to fatigue damage. E.g. vortex-induced vibrations (VIV) due to the wind, water impact on the jacket and vibrations due to slamming. There are three important methods for analyses of fatigue:

- Compute maximum accelerations in the cargo center of gravity (COG), and use them directly on the structural model of the cargo.
- Inertia loads are computed by applying a structural model of the cargo, and a hydrodynamic panel model of the barge.
- Inertia loads are computed by applying a combined model of barge and cargo.

The difference between the three methods is what they include in the analyses. For example, some include deflection of the vessel and some include acceleration components. This will give a difference in the results of the analyses (Bøe *et al.* , 2017).

2.1.2 Voyage sea states

To compute fatigue we need to know something about the sea state (waves, time of year, transportation route, etc.). Wave-induced inertia load is an important contribution to transportation fatigue. One problem that needs to be considered is that the roll damping becomes too large for smaller sea states and too low for higher sea states, when analyzing roll motions with todays guidelines.

We can not compute the roll motion for all wave directions, because it requires to much computation time. Hence we must find the most dominant sea state, when it comes to roll motion and the most probable wave direction at the route. The sea state should be conservatively assumed. We should note that the scatter diagrams are not a wave forecast, so the deviation of the sea state could be significant. According to (DNVGL-ST-N001, 2016), we should increase the transportation duration in the computations to compensate for this factor.

2.2 Roll damping

Roll damping is partly potential damping from radiating waves, and partly viscous damping from friction. The linear part of the damping can be determined

by diffraction-radiation calculations. More on this and potential theory in section 3.2.3. (Cozijn *et al.* , 2005)

The roll damping coefficient B44 is calculated in WADAM by including hydrodynamic effects from both potential damping and viscous damping. Potential damping is due to surface wave radiation and can be found by regular linear theory. The linear viscous damping includes contributions from bilge keel, skin-friction of the hull and eddy-making of the bilge keel. Damping effects from eddy-making due to the naked hull without the bilge keel is based on empirical data from Tanaka (Tanaka, 1960). The damping contributions from skin-friction and eddy-making from the bilge keel are calculated based on Kato's theory (Kato, 1966). These contributions are originally non-linear effects, but to be able to include it in the harmonic equation of motion for use in FD analysis the effects must be linearized (DNV-Software, 2005)

The Japanese scientists Ikeda, Himeno, Tanaka and Kato published many research papers on roll damping between the 60's and 80's. They came up with various components of damping as shown in the equation below (Falzarano *et al.* , 2015). These components are estimations of non-potential parts of the roll damping, also known as viscous damping, which is the most important contribution to the roll damping (Journée & Massie, 2001). (Ikeda *et al.* , 1978) came up with the following estimation formula for the equivalent damping.

$$B_{eq} = B_W + B_F + B_L + B_E + B_{BK} \tag{2.1}$$

Where
B_{eq} - Equivalent damping
B_W - Wave damping (Potential damping)
B_F - Friction damping
B_L - Lift damping
B_E - Eddy-making damping
B_{BK} - Bilge keel damping

Ikeda *et al.* (1978) made a plot with all the damping components, and their contributions depending on the speed of the vessel, shown in Figure 2.1.

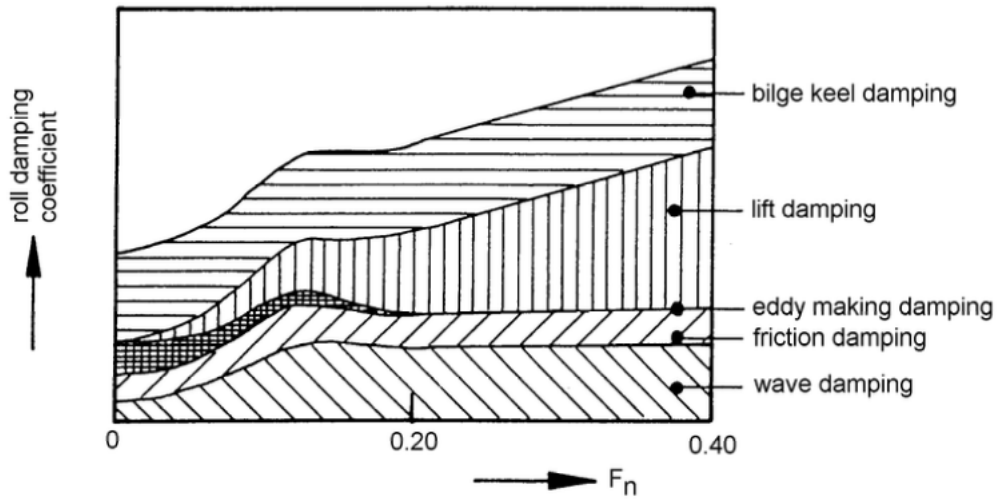

Figure 2.1: Viscous damping (Journée & Massie, 2001)

The speed of the vessel is expressed by the Froude number Fn given in the equation below.

$$Fn = \frac{U}{\sqrt{gL}} \tag{2.2}$$

Where U is the speed of the vessel, g is the gravity constant and L is the length of the vessel.

Equivalent damping - $\mathbf{B}_{eq}$

Equivalent damping is the total damping coefficient when all the damping components are added together, both potential and viscous. It is important to note that adding the components together is only valid for linear roll damping. The same components will be included in non-linear damping, but we need to find a different method to combine them to obtain the equivalent damping. More on that in section 3.4.

Wave damping - $\mathbf{B}_W$

Wave damping is caused by the free-surface waves. According to Ikeda *et al.* (1978) the wave damping at zero forward speed can be predicted accurately by strip theory. The results from experiments are confirming the calculations. When the vessel has forward speed, it gets more difficult. Ikeda *et al.* (1978) came up with an empirical formula based on a simple flow model. This method is later replaced by a more accurate panel method provided by the Norwegian scientist Salvesen. Wave damping is also known as potential damping and is not part of the viscous damping.

Friction damping - $\mathbf{B}_F$

The friction damping, also known as skin friction damping is drag caused by the viscous skin friction stress acting on the hull surface as the barge rolls (Falzarano *et al.* , 2015). Kato came up with a semi-empirical formula valid for laminar flow in 1958, but the barge experiences turbulent flow. Thus Tamiya et al. came up with a modification of Kato's formula (Ikeda *et al.* , 1978).

Lift damping - $\mathbf{B}_L$

Lift damping is due to a lift force, and the coefficient can be described by an empirical formulation deduced by (Ikeda *et al.* , 1978). The lift damping coefficient B_L varies linearly with the speed U and is independent of the roll motion frequency (Falzarano *et al.* , 2015). Due to the low speed of the barge during the transportation, we can assume the forward speed to be zero. Hence the contribution from lift damping is negligible.

Eddy-making damping - $\mathbf{B}_E$

The eddy-making damping is caused by flow separation and shedding of vortices around the bottom of the barge (Falzarano *et al.* , 2015). Flow separation leads to pressure variation on the hull, especially around the bilge keels. The pressure variation creates an eddy-making drag, which contributes to the roll damping (Chakrabarti, 2000). Eddy-making damping is a big part of the non-linear damping. In this case, the Eddy-making damping for zero forward speed is included, due to two reasons. First of all the barge, in this case, is assumed to have zero forward speed to simplify the problem. The second reason is that the eddy-making making damping is negligible at high speeds according to Figure 2.1.

Bilge keel damping - B_{BK}

The bilge keel damping is due to the resistance of the bilge keel through the water, and the pressure distribution around the body (Faltinsen, 1990). Bilge keel damping B_{BK} can be separated into two components, normal pressure damping B_{BKN} and hull damping B_{BKH} (Falzarano *et al.* , 2015).

$$B_{BK} = B_{BKN} + B_{BKH} \tag{2.3}$$

According to Ikeda *et al.* (1978) the normal force component of the bilge keels can be deduced from experimental results of oscillating flat plates. The hull damping is due to pressure on the hull surface created by the bilge keels. This component is deduced from experimental results fitted to an empirical formula. The calculations of the components using formulas is fairly good compared to experimental results.

In Figure 2.2 the vortex shedding from flow separation at the bilge keels is shown.

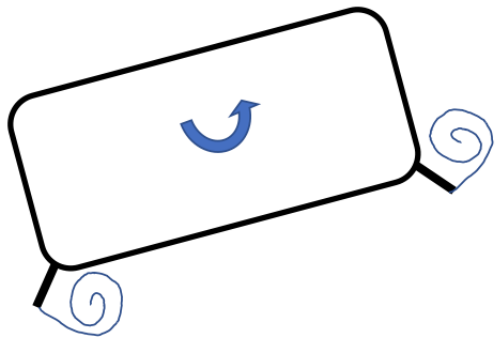

Figure 2.2: Bilge keel damping

As we can see from the illustration, the barge is rolling clockwise and creates a roll damping moment in the opposite direction.

Damping contributions included in WADAM calculations are from the follow-

ing hydrodynamic effects (damping effects). Potential damping from radiating waves and linearized viscous damping from skin-friction of the hull, eddy-making, and the bilge keel (DNVGL-Software, 2017).

2.2.1 Non-linear roll damping

When the roll motion exceeds 7-8^o it is no longer considered a linear motion, and we need to add a non-linear quadratic term and possibly also a cubic term. Only quadratic damping is considered in this project. Linearization of the non-linear term can be done in two ways, one method for regular sea and one method for irregular sea (Falzarano *et al.* , 2015). The quadratic damping term must be linearized, in order to solve the equation of motion in FD.

In WADAM it is possible to include a user-specified coefficient for quadratic damping. The coefficient can be obtained from e.g a model test. To be able to use it in FD analysis WADAM is linearizing the quadratic damping by using stochastic linearization.

The large roll motions increases the viscous damping. Viscous roll damping depends non-linearly on the roll motion response, and is therefore dependent on the sea state. The roll damping increases when the roll motion increases. The quadratic contribution comes from viscous effects, also known as drag, and are mainly a result of eddies. To calculate the viscous damping due to eddy-making for the naked hull we need to include a strip model. In this case the Tanaka/Kato method is used for the calculations, Integrations are performed to get the damping along the total barge length. Calculations of viscous damping from the bilge keel uses the same strip model as for the previous contribution. The dimensions of the barge is defined in HydroD and is transferred to the WADAM analysis.

When the stochastic linearization is used to find the linear damping term, the maximum roll angle defined in HydroD will be the input in the first iteration. To obtain a satisfying result the convergence criteria must be less than 0.1%. The stochastic linearization can only be used in a short-term sea state. If we want to find the linearized roll damping for a long-term sea state manual iterations is required (DNVGL-Software, 2017).

2.2.2 Breadth-draught ratio and damping

In this section we are going to look at how the breadth-draught ratio of a cross section of a barge affect the damping coefficient. The relation between the roll damping and the breadth-draft ratio is given in Figure 2.3.

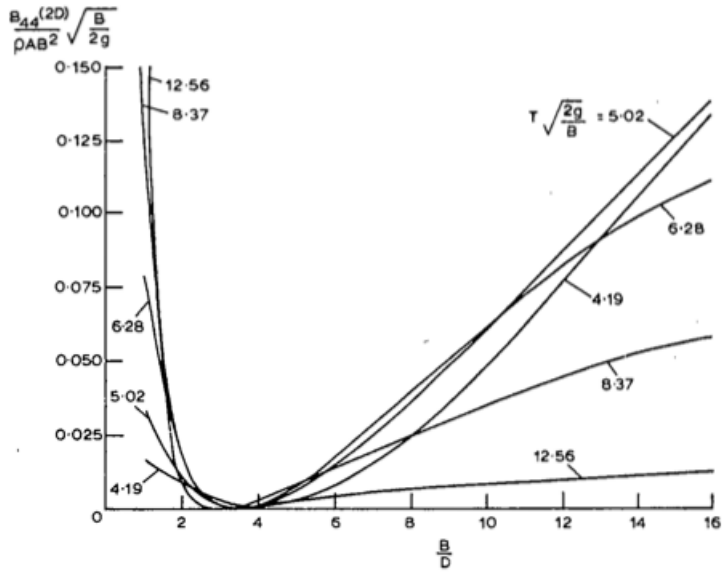

Figure 2.3: Breadth-draught ratio vs damping

For very low and high breadth-draught ratios the roll damping coefficient is very high, and it has its minimum at about 3-4. For barges this is important to include this damping contribution due to its high breadth-draught ratio.

2.2.3 Devices to reduce roll motion

To reduce the wave-induced fatigue damage on the cargo, we can try to minimize the roll motion, especially the resulting translational acceleration and inertia loads. For this purpose, we can add mechanisms that contribute to the roll damping. We divide the mechanisms into two groups, active and passive

mechanisms. Active mechanisms are, e.g. active fins, gyrostabilizer, and adjustable weights, mechanisms that need an external influence to work properly. While the passive mechanisms counteract the roll motion by itself, e.g. bilge keel, roll tanks, and fixed fins. Bilge keels, Anti-roll tank stabilizers, and active fins are the most effective mechanisms (Falzarano *et al.* , 2015).

Bilge keel

The bilge keels are a passive mechanism attached to the bilge at each side of the barge as illustrated in Figure 2.4. In the longitudinal direction, the bilge keel extends up to half the length of the ship, and its purpose is to reduce the roll motion. This is one of the most common mechanisms to damp the roll motion, because it is effective at both zero and non-zero forward speed. The damping occurs due to viscous damping, more on that later in the report. An illustration of the barge with bilge keels is illustrated in Figure 2.4.

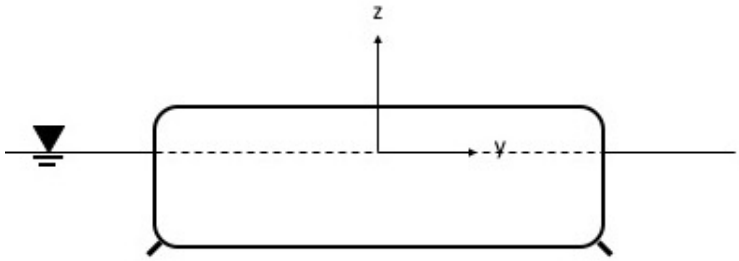

Figure 2.4: Bilge keel

Anti-roll tank stabilizers

Two types of anti-roll tank stabilizers are illustrated in Figure 2.5. The figure to the left illustrates a free surface tank, and the figure to the right illustrates a U-tube tank.

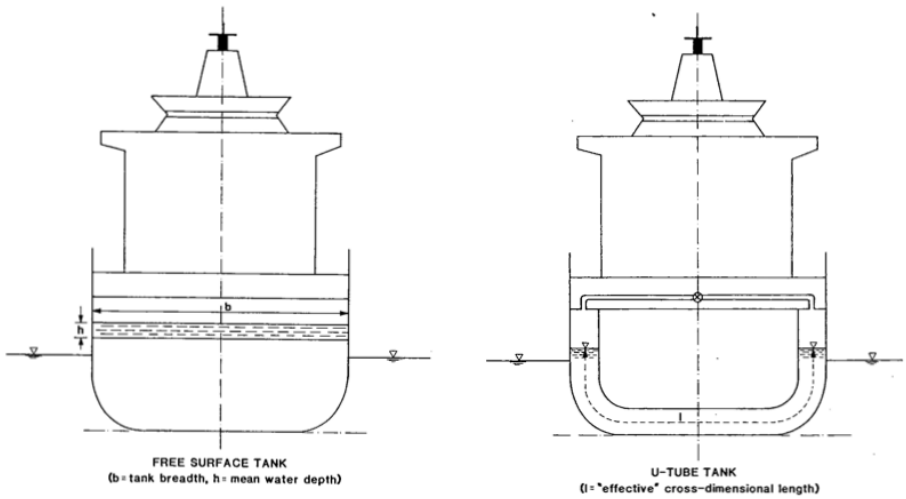

Figure 2.5: Passive anti-roll tank stabilizers (Faltinsen, 1990)

The principle behind this damping system is a roll moment caused by the anti-roll tank are damping the roll motion. The anti-roll tank system works best if the natural period of the tank is close to the natural period of roll motion. By changing the water level in the tank, we can change the period of the fluid motion, and make it closer to the natural period of roll motion. When the two periods are close to each other, the tank moment is about 180^o out of phase to the roll velocity. This causes a stabilizing moment, and are reducing the roll motion (Faltinsen, 1990).

An example of the response of the ship in roll motion with and without anti-roll tank stabilizers are presented in Figure 2.6.

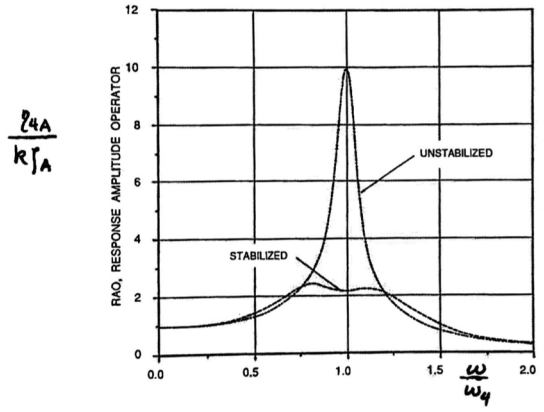

Figure 2.6: Roll motion with and without passive tank stabilizers (Pettersen, 2007)

As we can see the mechanism works very well around the resonance frequency. The response amplitude operator (RAO) when the frequency is equal to the natural frequency in roll motion is significantly reduced. Outside the resonance domain, the anti-roll tank stabilizers do not reduce the roll motion, rather the contrary, which is why we need the natural frequency in the tank to be almost the same as the natural frequency in roll motion.

Fins

Fins can be both passive and active, the most common application of fins are at cruise ships to make the voyage more comfortable for the passengers. The active fins can be adjusted to counteract the motions in the best way.

The most important roll motion reducing mechanism for barges is the bilge keel. The mechanism works good for both zero and non-zero forward speed, which is important for the barge.

We found out that bilge keels gives the best reduction in roll motion. In this case the damping comes from the force directly on on the bilge keels, and the difference in pressure between the two sides of the bilge keel. Normally we say that half of the damping is caused by the bilge keels. It is also a damping effect from lift in the hull which varies depending on the speed, higher speed gives

higher a higher damping factor, The speed in our case is low, hence this will not be considered.

2.2.4 Frequency domain vs Time domain analysis

Frequency domain analysis

Frequency domain analysis is defined as the process of analyzing large volume structures in regular incident waves. In reality, the waves are irregular and must be divided into regular wave components. The regular wave components are used to analyze both motions and forces. Frequency domain analysis is a linear analysis, which means that we are focusing on first order wave loads. When the output is proportional to the input, we have linearity. In wave load theory this is defined as resulting loads, and dynamic pressure is proportional to the wave amplitude (DNV-RP-H103, 2011).

The results from a linearization of roll damping are not perfect, but the results are usually precise enough to be applied in fatigue analyses. The advantage with frequency domain analyses is that the computations are fairly simple and efficient compared to time domain analysis (DNV-RP-H103, 2011).

Time domain analysis

While some loads can be linearized and used in frequency domain analysis, other loads of higher order cannot be linearized. In the cases where the loads can not be linearized, we need to use time domain analysis. The advantage of this method is that it can include non-linear hydrodynamic load effects. TD analysis involves numerical integration of the equation of motion, and is used when non-linear effects are important, it is usually applied for predictions of extreme load effects. To find out if the non-linear effects are significant for roll damping we are comparing frequency domain analysis and time domain analysis. If the results are considered as close enough, it is easier and less time consuming to do the analysis in frequency domain (DNV-RP-H103, 2011).

Chapter 3

Theory

This chapter intends to present the theoretical background necessary for this thesis. It includes theory used for obtaining input variables, some of the main theory behind HydroD/WADAM and the theory used in post-processing.

3.1 Coordinate system

When describing the motions of the barge, we use the Greek letter η to describe the six Degrees of Freedom (DoF). $\eta = [\eta_1\ \eta_2\ \eta_3\ \eta_4\ \eta_5\ \eta_6]^T$ represents the motion in surge, sway, heave, roll, pitch and yaw, respectively. An illustration of the DoF is shown in the Figure 3.1.

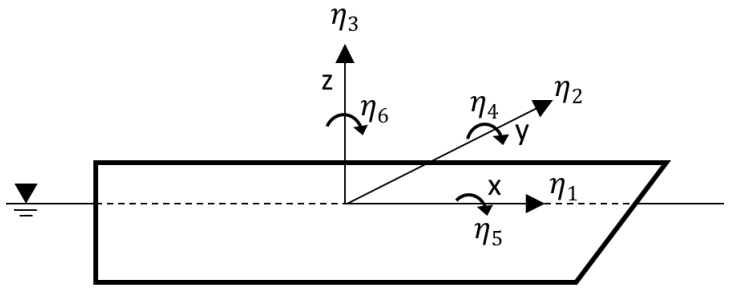

Figure 3.1: Coordinate system

As we can see from the figure, surge, sway, heave are components of translation, while roll, pitch, and yaw are components of rotation. Roll is coupled to sway and yaw, but we consider this problem as uncoupled to simplify the calculations. The origin is vertically located at the still water level (SWL), horizontally at the center line and COG in the longitudinal direction.

3.2 Wave theory

The response of a vessel is mainly due to waves, thus the theory of waves is essential to establish. First of all wave spectra will be explained, this is used for describing the sea states. The response depends on the excitation forces acting on the vessel. The excitation depends on the sea state, which is a function of wave height, period and direction. After that, the method for obtaining excitation forces will be presented through potential wave theory and the radiation and diffraction problem.

3.2.1 Wave spectrum

A wave spectrum is a representation of a sea state based on the energy amount. The energy in the spectrum should be the same as for the real sea state. Wave spectra are usually based on real measurements from one location, presented in a scatter diagram. An example of a scatter diagram is presented in Appendix 6.3.

It is difficult to get the actual wave spectrum for a specific area, especially when we are talking about transportation where the location is not fixed. In this case, there are developed some standardized wave spectra for different areas in the world. They are used to calculate the response for a structure in a specific location. It is important to note that the standardized wave spectra is sort of a mean wave spectra, which must be accounted for when calculating responses.

For the response calculations in this thesis, a JONSWAP spectrum is used. JONSWAP stands for Joint North Sea Wave Project and is derived from a Pierson-Moskowitz (PM) spectrum.

Pierson-Moskowitz

A PM spectrum is based on data from the North Atlantic Ocean and is given by the following shape.

$$S(\omega) = \frac{A}{\omega^5} exp\left[-\frac{B}{\omega^4} \right] \tag{3.1}$$

Where $S(\omega)$ is the wave spectrum, as a function of the wave frequency ω. The unit of a wave spectrum is $[m^2 s]$. A and B are parameters given by Equation 3.2 and 3.3.

$$A = 0.0081 g^2 \tag{3.2}$$

$$B = 0.74 \left(\frac{g}{V} \right)^4 \tag{3.3}$$

Where g is the gravity constant, and V is the wind velocity which in the PM spectrum acts as the only parameter.

The spectrum will go towards a curve given by ω^{-5} when the wave frequencies goes towards infinity. According to Phillips (1958) this is a property common for all wave spectra and describe a fully developed wave spectra. (Myrhaug, 2004)

JONSWAP

The JONSWAP spectrum was developed as result of a multinational measurement project where they found out that the measurements in the North Sea gave very pointed peak. JONSWAP is based on PM, but instead of having the main focus on the wind velocity, JONSWAP has its main focus on the top frequency ω_p. If a PM and JONSWAP spectrum are used to describe the same sea state, the total energy will be the same for both of them, but the energy distribution is different. A JONSWAP spectrum has more energy around the top frequency, and less further away from the top frequency compared to a PM spectrum. A JONSWAP spectrum can be described by 4 parameters (ω_p, α, γ, σ), we can alternatively include the significant wave height H_S and the zero up-crossing period T_Z. The spectrum is given by Equation 3.4.

$$S(\omega) = \alpha g^2 \omega^{-5} exp\left(\frac{-5}{4} \left(\frac{\omega}{\omega_p} \right)^{-4} \right) \gamma^a \tag{3.4}$$

Where the peakedness γ is ratio between max energy in JONSWAP and PM. The variable a is shown in Equation 3.5

$$a = exp\Big(-\frac{1}{2}\Big(\frac{\omega - \omega_p}{\sigma\omega_p}\Big)^2\Big) \tag{3.5}$$

Where σ describes the width of the spectrum, and is divided into σ_a and σ_b to describe the width of each side of the peak frequency DNVGL-Software (2016) and (Hasselmann *et al.* , 1973).

In Figure 3.2 the range of the JONSWAP spectrum is illustrated. The range is between the two lines, if γ is 1, JONWAP and PM have equal peakedness.

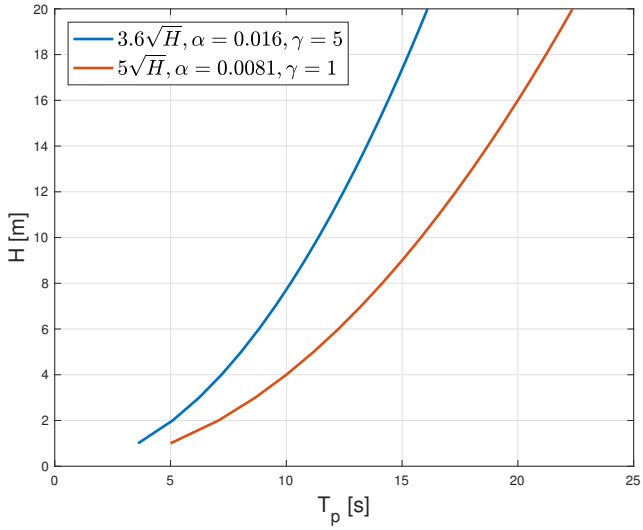

Figure 3.2: JONSWAP range

An example of a JONSWAP spectrum is illustrated in Figure 3.3.

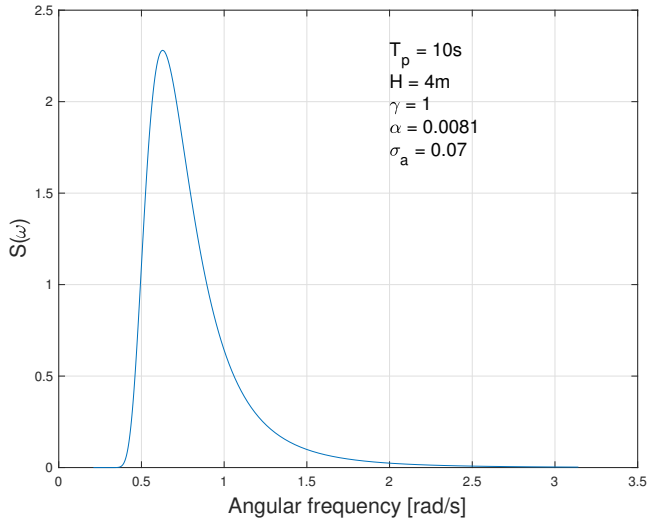

Figure 3.3: JONSWAP spectrum

It is two ways to define the period in a spectrum. First one is defined by the peak period T_p, and the other one is by the zero up-crossing period T_z. The relation between them defined in WADAM is presented in Equation 3.6

$$T_z = 0.777T_p \tag{3.6}$$

3.2.2 Potential wave theory

To get a better understanding of how wave loads are acting on ships we need to establish the basis for calculating wave loads. The theory in this section is based on theory from the book: *Sea Loads On Ships And Offshore Structures* (Faltinsen, 1990). There are other sea loads in addition to wave loads, e.g. wind and currents, but they will not be considered in this thesis.

By using potential theory, we can describe the fluid with a potential velocity ϕ, as described in Equation 3.7. From the velocity potential, we can obtain the velocity and acceleration of the fluid, the pressure by using Bernoulli's equation, and the wave elevation ζ. To be able to apply potential theory we need to establish some basic assumptions. The sea water must be incompressible and inviscid, and the fluid motion must be irrotational. $\mathbf{V}$ is the velocity vector at

time t and point (x,y,z) and can be written as follows.

$$\begin{gathered}\mathbf{V}(x,y,z,t) = (u,v,w) \\ \mathbf{V} = \nabla\phi \equiv \mathbf{i}\frac{\partial\phi}{\partial x} + \mathbf{j}\frac{\partial\phi}{\partial y} + \mathbf{k}\frac{\partial\phi}{\partial z}\end{gathered} \tag{3.7}$$

Where **i**, **j** and **k** are unit vectors in x-, y- and z-direction respectively.

From Equation 3.8 we have the vorticity vector. For an irrotational fluid this is equal to zero everywhere in the fluid.

$$\boldsymbol{\omega} = \nabla \times \mathbf{V} \tag{3.8}$$

Where, $\boldsymbol{\omega}$ is the vorticity vector.

Since we assume the water to be incompressible $\nabla \cdot \mathbf{V} = 0$, the velecoty potential must satisfy the Laplace equation given in Equation 3.9

$$\nabla \cdot \mathbf{V} = \frac{\partial^2\phi}{\partial^2 x} + \frac{\partial^2\phi}{\partial^2 y} + \frac{\partial^2\phi}{\partial^2 z} = 0 \tag{3.9}$$

The velocity potential of an irrotational, incompressible fluid motion is obtained by solving the Laplace equation with relevant boundary conditions which will be shown later in this section.

Equation 3.10 is Bernoulli's equation and is used to find the pressure p in the fluid. We assume positive z-axis upwards, and $z = 0$ at free-surface.

$$p - p_a = -\rho g z - \rho\frac{\partial\phi}{\partial t} - \frac{\rho}{2}\mathbf{V}\cdot\mathbf{V} \tag{3.10}$$

Where p_a is the ambient pressure. The first term on the right side of the equation is the static term, the two remaining terms are the dynamic linear and quadratic term. The pressure distribution in the fluid obtain by Equation 3.10 is important to know to be able to find the forces acting on the structure.

Boundary conditions

To obtain a velocity potential that correctly describes the fluid we need to include some boundary conditions. There are three types of boundary conditions, kinematic boundary condition, kinematic free-surface condition, and dynamic free-surface condition. Figure 3.4 illustrates the boundary conditions for a barge, which is going to be explained in this section.

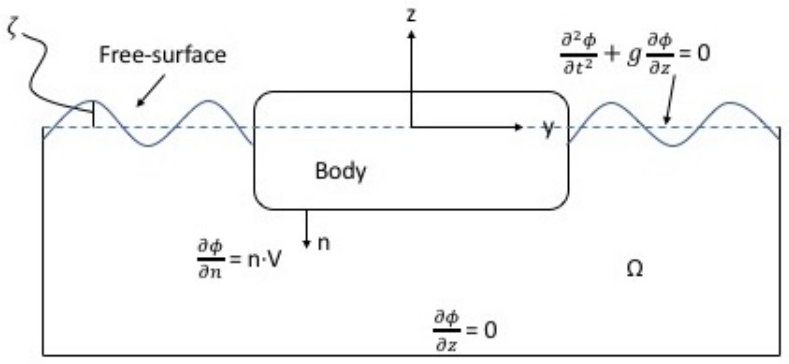

Figure 3.4: Boundary conditions

Where Ω is the fluid domain and n is the normal to the body surface. The body surface is the wetted part of the structure.

Equation 3.11 is the body boundary condition and expresses the impermeability, which means that no fluid enters or leaves the body surface

$$\frac{\partial \phi}{\partial n} = \mathbf{U} \cdot \mathbf{n} \tag{3.11}$$

Where **U** is the velocity of the body. Since we are assuming that the barge has zero forward speed we can put Equation 3.11 equal to 0. This means that the body is fixed and only the fluid is moving.

From Equation 3.12 we have the kinematic free-surface condition, which states

that the fluid particles on the free-surface remain there.

$$\frac{\partial \zeta}{\partial t} + \frac{\partial \phi}{\partial x}\frac{\partial \zeta}{\partial x} + \frac{\partial \phi}{\partial y}\frac{\partial \zeta}{\partial y} - \frac{\partial \phi}{\partial z} = 0 \qquad on \quad z = \zeta(x, y, t) \tag{3.12}$$

Equation 3.13 describes the dynamic free-surface condition, where the water pressure is equal to the constant ambient pressure p_a. We are usually saying that the ambient pressure is the atmospheric pressure. This can be expressed by Bernoulli's Equation 3.10.

$$g\zeta + \frac{\partial \phi}{\partial t} + \frac{1}{2}\left[\left(\frac{\partial \phi}{\partial x}\right)^2 + \left(\frac{\partial \phi}{\partial y}\right)^2 + \left(\frac{\partial \phi}{\partial z}\right)^2\right] = 0 \qquad on \quad z = \zeta(x, y, t) \tag{3.13}$$

To simplify the calculations we can linearize the problem, then the response will be proportional to excitation. Which means that the body-motion amplitude is proportional to the incident wave amplitude. The linearization is done by Taylor expansion of the boundary conditions and the results are shown in Equation 3.14 and 3.15, and represents the result at the mean free-surface where $z = 0$. Equations 3.14 is the kinematic condition and 3.15 is the dynamic condition.

$$\frac{\partial \zeta}{\partial t} = \frac{\partial \phi}{\partial z} \tag{3.14}$$

$$g\zeta + \frac{\partial \phi}{\partial t} = 0 \tag{3.15}$$

If we differentiate Equation 3.15 with respect to time we can obtain the combined free surface condition 3.16 by substituting 3.15 into 3.14.

$$\frac{\partial^2 \phi}{\partial t^2} + g\frac{\partial \phi}{\partial z} = 0 \qquad on \quad z = 0 \tag{3.16}$$

The theory described in Section 3.2.2 is implemented in WADAM for calculations of first-order radiation and diffraction effects on large structures (DNVGL-Software, 2017).

3.2.3 Linear hydrodynamic loads

The first contribution to damping is the linear hydrodynamic loads, based on potential theory. First of all, we want to find the solution of the wave-body interaction problem in terms of the potential ϕ. (Greco, 2012) The incoming

waves are known, and we assume linearity and steady state conditions to be able to solve it in the frequency domain. Due to linearity, it is valid to use the superposition principle, and we decompose the potential ϕ into two sub-problems diffraction- and radiation problem. The result is linear hydrodynamic loads, as shown in the Figure 3.5.

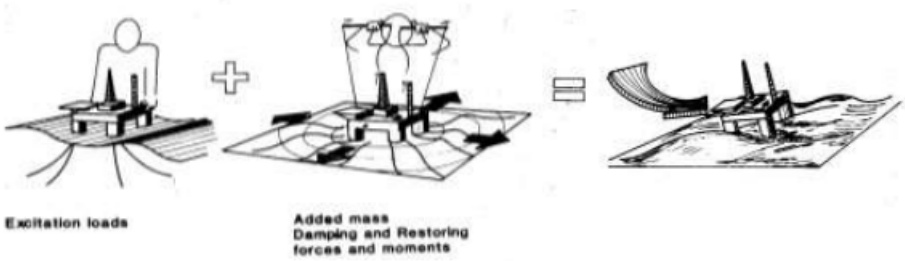

Figure 3.5: Linear hydrodynamic loads (Faltinsen, 1990)

Figure 3.5 illustrates the two sub-problems. The first term is the diffraction problem, and the second term is the radiation problem. These two terms added together becomes; linear wave-induced motions, accelerations and structural loads (Faltinsen, 1990).

Diffraction problem

The aim of this problem is to find the excitation loads. In the diffraction problem, the structure is restrained from motions and is excited by incident waves. It is divided into two potentials, diffraction and incident waves, and added together to solve the velocity potential.

$$\phi(x, y, z, t) = \phi_0(x, y, z, t) + \phi_D(x, y, z, t) \tag{3.17}$$

Where $\phi(x, y, z, t)$ is the velocity potential, $\phi_0(x, y, z, t)$ is due to incident waves, and $\phi_D(x, y, z, t)$ is the diffraction.

We are splitting the velocity potential into two problems as shown in the Figure 3.6.

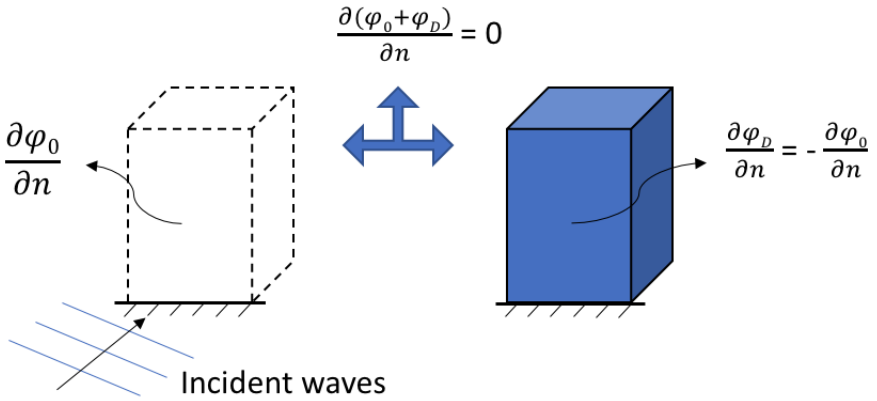

Figure 3.6: Diffraction problem

In the left figure, the waves penetrate the body with a normal velocity $\partial\phi_0/\partial n$ like the body was not there. This causes hydrodynamic loads on the body, called Froude-Krylov loads. To recover the body impermeability, we include an elastic body with normal velocity in the opposite direction of ϕ_0. The hydrodynamic loads caused by the compensation for the incident wave disturbance is called diffraction loads. The excitation force is found by adding the Froude-Krylov loads and the diffraction loads, by integrating the dynamic pressure from the incident waves and diffraction along the mean wetted surface. The result is shown in the equation below.

$$F_{exc}(t) = -\int_S \rho \frac{\partial \phi_0}{\partial t} n dS - \int_S \rho \frac{\partial \phi_D}{\partial t} n dS \tag{3.18}$$

Where F_{exc} is the wave excitation load and ρ is the water density. The first term is Froude-Krylov loads, and the second term is diffraction loads (Faltinsen, 1990).

Radiation problem

For the radiation problem, also known as the added mass problem, the structure is forced to oscillate in its 6 DoF with the wave frequency ω. There are no incident waves, and the velocity potential solving this problem is given by the equation below.

$$\phi(x, y, z, t) = \phi_R(x, y, z, t) \tag{3.19}$$

Where $\phi_R(x, y, z, t)$ is the radiation potential representing the waves generated, radiating outwards.

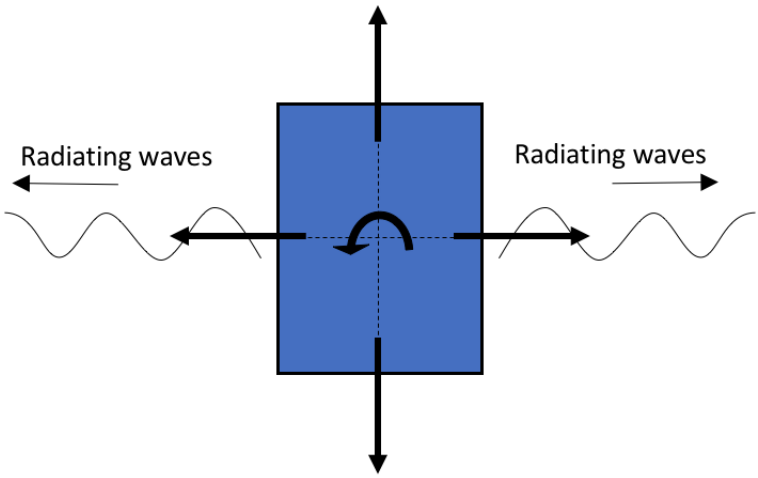

Figure 3.7: Radiation problem

The velocity potential can be split into 6 sub-problems.

$$\phi_R(x, y, z, t) = \sum_{j=1}^{6} \dot{\eta}_j \phi_j \tag{3.20}$$

The hydrodynamic loads are identified as added mass, damping and restoring terms. Added mass and damping are due to dynamic pressures caused by body motion, and the restoring force is due to variation in buoyancy. To obtain the

force on the body due to radiation potential, we need to integrate the pressure over the mean wetted surface as shown in the equation below.

$$F_{rad}(t) = -\int_S \rho \frac{\partial \phi_R}{\partial t} n dS \tag{3.21}$$

Where $F_{rad}(t)$ is the radiation load

When the radiation and diffraction problem is solved we express the total wave potential as the sum of the diffraction- and radiation problem.

$$\phi(x, y, z, t) = \phi_0(x, y, z, t) + \phi_D(x, y, z, t) + \phi_R(x, y, z, t) \tag{3.22}$$

For large floating structures in waves the diffraction/radiation problem is used to calculate the damping. For most of the DoF this is a good prediction of the damping, but for roll motion of a long floating structure, e.g. barges, the radiation damping is quite small compared to the total damping. This is due to the highly non-linear damping in roll motion (Chakrabarti, 2000). This is why we are using the empirical formulas that Ikeda *et al.* (1978) came up with based on experimental data.

3.3 Equation of motion

Roll damping is a phenomenon related to the motions of the system, hence we begin with the equation of motion for 6 DoF. Normally we are using a statistical analysis when analyzing the barge motions. For linear systems, we perform the analyses in FD and non-linear systems in a TD (Natskår & Moan, 2010). The equation of motion is derived from Newton's second law.

3.3.1 Frequency domain

In FD the equation of motion is a function of frequency, and it is described by the sum of the equation of motion for each DoF. For each DoF, we need to include the contribution from all the other DoFs. The equation of motion is expressed in Equation 3.23

$$\sum_{k=1}^{6} [(M_{jk} + A_{jk}(\omega))\ddot{\eta}_k + B_{jk}(\omega)\dot{\eta}_k + C_{jk}\eta_k] = F_j(\omega) \qquad (j = 1, ..., 6) \tag{3.23}$$

Where M is the mass of the barge including the jacket, $A(\omega)$ is the added mass, η_4 is the motion in roll. $B(\omega)$ is the damping, C is the restoring term, ω is the angular frequency of the incident waves, $F_4(\omega)$ is the excitation moment. To avoid the time dependence we may use complex notation, more on this in Section 3.3.2.

The equation of motion can be simplified because some of the motions are not coupled, no coupling effect means that they are not giving any motion contribution to each other. There are no coupling effects between the lateral motions (roll, sway and yaw) and the longitudinal and the vertical motions (surge, pitch and heave). Hence, when studying roll motion we only need to consider coupling effects from sway and yaw. To simplify the computations even more we are assuming no coupling effects for the roll motion. Thus we can define the equation of motion for roll motion as shown in Equation 3.24

$$(M + A(\omega))\ddot{\eta_4} + B(\omega)\dot{\eta_4} + C\eta_4 = F_4(\omega) \tag{3.24}$$

From the linear equation of motion 3.24 we can add a quadratic damping term B_2, making the damping non-linear, as shown in Equation 3.25

$$(M + A)\ddot{\eta}_4 + B_1\dot{\eta}_4 + B_2|\dot{\eta}_4|\dot{\eta}_4 + C\eta_4 = F_4 \tag{3.25}$$

Where $B_2|\dot{\eta}_4|\dot{\eta}_4$ is the quadratic damping term

3.3.2 Time domain

Since Newton's laws applies in time domain we have a function of t, and we may express the excitation force as F(t). Corresponding to Equation 3.25 in FD we can define the non-linear equation of motion in TD as presented in Equation 3.26.

$$(M + A_\infty)\ddot{\eta_4} + B_2|\dot{\eta_4}|\dot{\eta_4} + C\eta_4 + \int_0^t h(t-\tau)\dot{\eta_4}(\tau)d\tau = F_4(t) \tag{3.26}$$

Where, A_∞ is $\lim_{\omega\to\infty} A(\omega)$, τ is a time variable not to be confused with t, and $h(\tau)$ is the retardation function matrix, it may be calculated from the frequency dependent damping, or from the added mass (Natskår & Steen, 2013).

3.3.3 Excitation forces

All transfer functions for exciting forces and moments are calculated by solving the diffraction problem and by applying the Haskind relation on the radiation potentials. Haskind relation can be used if we only want to find the wave excitation loads when the detailed pressure distribution is not of importance. In general, the Haskind relation is used to check the accuracy of the software (DNVGL-Software, 2017).

3.3.4 Response

From the equation of motion 3.24 in frequency domain we can obtain the response in roll motion for the barge. The first step is to express the equation of body motion by the roll amplitude η_{4a} by substituting harmonic equations as follows.

$$\eta_4 = \eta_{4a} e^{i\omega t} \tag{3.27}$$

$$\dot{\eta}_4 = i\omega \eta_{4a} e^{i\omega t} \tag{3.28}$$

$$\ddot{\eta}_4 = -\omega^2 \eta_{4a} e^{i\omega t} \tag{3.29}$$

Assuming the problem to be steady state, the equation of motion can be written without including the time.

$$[-\omega^2(M + A) + i\omega B + C]\eta_{4a} = F_4 \tag{3.30}$$

When calculating the response we can either solve the differential Equation 3.24 or we can solve it by using a transfer function. The transfer function is defined by a Laplace transform, where the excitation force is the input and the response as the output. For the equation of motion we can define the transfer function $H(\omega)$ as presented in Equation 3.31.

$$H(\omega) = \frac{\eta_{4a}}{F_4} \tag{3.31}$$

By inserting Equation 3.30 into 3.31 the transfer function $H(\omega)$ can be expressed as follows.

$$H(\omega) = [-\omega^2(M + A) + i\omega B + C]^{-1} \tag{3.32}$$

Now that we have the transfer function we can use a wave spectrum as described in Section 3.2.1 to obtain the response. The response spectrum can be calculated the following relation in frequency domain defined by Equation 3.33.

$$S_{\eta 4}(\omega) = |H(\omega)|^2 S(\omega) \tag{3.33}$$

Where $S_{\eta 4}(\omega)$ is the response spectrum (Ochi, 1990).

3.3.5 Motion

The motion at any point on the barge can be described by Equation 3.34.

$$\mathbf{s} = (\eta_1 + z\eta_5 - y\eta_6)\mathbf{i} + (\eta_2 - z\eta_4 + x\eta_6)\mathbf{j} + (\eta_3 + z\eta_4 - x\eta_5)\mathbf{k} \tag{3.34}$$

Where **i**, **j** and **k** are the unit vectors along the x-, y- and z-axis, respectively.

Acceleration

In fatigue calculations, we are focusing on the acceleration due to the viscous roll damping, since this is the main contribution to fatigue. Acceleration in the longitudinal direction is independent of the roll motion, and the acceleration in vertical directing is assumed to be small compared to the acceleration in the horizontal direction. Thus, we are considering only acceleration in the transverse direction. From Equation 3.29, we can write the transverse acceleration due to inertia as a^*_{tra}.

$$a^*_{tra} = -\omega^2 L \tag{3.35}$$

Where L is the distance from centre to the fastening point.

By including the contribution from the gravity, the total wave induced transverse acceleration can be expressed as follows.

$$a_{tra} = a^*_{tra} + g\eta_4 \tag{3.36}$$

The acceleration computed can be included in the fatigue analysis. (Yang *et al.*

, 2018). To be able to compare with the TD analysis, we compare the response spectrum for acceleration shown in Equation 3.37.

$$S_{\ddot{\eta}}(\omega) = |\omega^2 L|^2 S_{\eta 4}(\omega) \tag{3.37}$$

Where, $S_{\ddot{\eta}}(\omega)$ is response spectrum in terms of acceleration.

3.4 Equivalent linearization technique

The equivalent linearization technique is the most common method used to obtain the solution of a non-linear system. The principle of this method is to express the non-linear equation of motion in a linear form. We can do that by considering an equivalent balance of energy during one cycle such that the work for each cycle is the same for the two systems. When investigating non-linear roll damping, we are dealing with a non-linear system with random excitation. Thus a method to evaluate the root mean square value of the response is established, where we consider the minimization of the error associated with the linear transformation (Ochi, 1990).

From the non-linear equation of motion presented in Equation 3.25 we can derive an expression for the equivalent linear damping term for both regular waves and irregular waves.

Regular waves

To be able to do computations in FD we need to linearize the non-linear damping term. Thus we introduce a new linear damping term where the energy loss for the linear equation shall be the same as the real energy loss per cycle. We call this term the equivalent damping, and the equilibrium is presented below (Langen & Sigbjornsson, 1979)

$$\int_0^T B_{eq}\dot{\eta}_4 \frac{\partial \eta}{\partial t} dt = 4 \int_0^{\frac{T}{4}} B_2 |\dot{\eta}_4| \dot{\eta}_4 \frac{\partial \eta}{\partial t} dt \tag{3.38}$$

Where B_{eq} is the equivalent damping.

We are integrating over one period, but as we can see from the term on the

right side, we are integrating over a quarter period. Otherwise the right side of the equilibrium will become 0. Since we are integrating from 0 to T/4, we need to multiply the integral by 4 to achieve the contribution from one period T.

In hydrodynamic calculations we are usually using the angular frequency ω instead of the period T. The relationship between T and ω is defined in Equation 3.39.

$$T = \frac{2\pi}{\omega} \tag{3.39}$$

Next we introduce the real part of a harmonic motion expressed in Equation 3.40.

$$\eta_4 = \eta_{4A} sin(wt) \tag{3.40}$$

Where, η_{4A} is the roll amplitude

If we insert Equation 3.40 into 3.38 we get the following equation.

$$B_{eq}\omega^2\eta_{4A}^2 \int_0^{\frac{2\pi}{\omega}} cos^2(\omega t)dt = B_2\omega^3\eta_{4A}^3 4 \int_0^{\frac{\pi}{2\omega}} cos^3(\omega t)dt \tag{3.41}$$

This results in

$$B_{eq}\omega^2\eta_{4A}^2\frac{\pi}{\omega} = B_{eq}\omega^3\eta_{4A}^3\frac{8\pi}{3\omega} \tag{3.42}$$

Which is rearranged to

$$B_{eq} = \frac{8}{3\pi}\omega\eta_{4A}B_2 \tag{3.43}$$

Now we can write the total linearized damping term by including the original linear damping shown in equation 3.44.

$$B_{eq} = B_1 + \frac{8}{3\pi}\omega\eta_{4A}B_2 \tag{3.44}$$

(Pettersen, 2007)
Since the roll damping dominates the roll motion around the resonance frequency, the natural roll period for the barge is important for the wave damping. The uncoupled natural period for the barge is presented in Equation 3.45.

$$T_{n4} = 2\pi \left(\frac{Mr_{44}^2 + A_{44}}{\rho g V G M_T} \right)^{\frac{1}{2}} \tag{3.45}$$

Where r_{44} is the roll radius of gyration, A_{44} is the added moment in roll, V is the displaced volume of the barge and GM_T is the transverse metacentric height.

Irregular waves

Irregular waves are the sum of regular waves with a different period, amplitude, and phase, and is what we call a stochastic process. Since the incident waves are simplified to be a random process, the excitation force F_x is a random process, hence is difficult to obtain an exact solution of the motion $\eta(t)$. Since $\eta(t)$ is an approximation it is more relevant to look at the probability distribution of the amplitude of the response.

For irregular roll motion, we need to use another approach to linearize the roll damping term. We assume that the difference between the damping for the linearized term and the real value can be minimized by the least square method. The error ε associated with the linearization is expressed in Equation 3.46.

$$\varepsilon = B_1\dot{\eta}_4 + B_2|\dot{\eta}_4|\dot{\eta}_4 - B_{eq}\dot{\eta}_4 \tag{3.46}$$

We want determine the damping coefficient such that the error is as small as possible. One way to minimize ε is by the mean square value $\mathrm{E}[\varepsilon^2]$. First of all we need to see if it is possible to minimize $\mathrm{E}[\varepsilon^2]$ by application of Equation 3.47

$$\frac{\partial^2}{\partial B_{eq}^2} E[\varepsilon^2] = 2E[\dot{\eta}^2] > 0 \tag{3.47}$$

If the requirement are fulfilled, it is possible to minimize $\mathrm{E}[\varepsilon^2]$ by Equation 3.48

$$\frac{\partial}{\partial B_{eq}} E[\varepsilon^2] = 0 \tag{3.48}$$

Minimization of the mean squared value $E[\varepsilon^2]$ is expressed in Equation 3.49. This is only valid if we assume a Gaussian random process, and that the damping coefficients B_{eq}, B_1 and B_2 remains constant.

$$\frac{\partial}{\partial B_{eq}} E[\varepsilon^2] = -2(B_1 - B_{eq})E[\dot{\eta}_4^2] - 2B_2 E[\dot{\eta}_4^2|\dot{\eta}_4|] = 0 \tag{3.49}$$

Expressed by B_{eq} we get the formulation in Equation 3.50.

$$B_{eq} = B_1 + B_2 \frac{E[|\dot{\eta}|^3]}{E[\dot{\eta}^2]} \tag{3.50}$$

Since we are assuming a Gaussian process and the mean value is zero, we can write the unknown variance of the roll motion $\dot{\eta}$ as shown in Equation 3.51.

$$\begin{aligned} E[\dot{\eta}^2] &= \sigma_{\dot{\eta}}^2 \\ E[|\dot{\eta}|^3] &= \frac{2\sqrt{2}}{\sqrt{\pi}} \sigma_{\dot{\eta}}^3 \end{aligned} \tag{3.51}$$

Inserted into Equation 3.50 we get

$$B_{eq} = B_1 + 2\sqrt{\frac{2}{\pi}} \sigma_{\dot{\eta}_4} B_2 \tag{3.52}$$

Where $\sigma_{\dot{\eta}_4}$ is the standard deviation of the response $\dot{\eta}_4$.
Furthermore we express the variance, which is the standard deviation squared, as shown in Equation 3.53.

$$\sigma_{\dot{\eta}_4}^2 = 2 \int_0^\infty S(\omega)|H(\omega)|^2 d\omega \tag{3.53}$$

Where $S(\omega)$ is the wave spectrum, and $|H(\omega)|^2$ is the squared transfer function known as the RAO (Response amplitude operator). The RAO is defined as the motion amplitude divided by the wave elevation amplitude.

Based on a Rayleigh probability function we approximate the maxima, and

the most probable largest value of the response, R_{max} is expressed by the following equation.

$$R_{max} = (2\sigma^2_{\dot{\eta}_4} log\frac{t}{T})^{\frac{1}{2}} \tag{3.54}$$

(Hemeno, 1981), (Ochi, 1990) and (Faltinsen, 1990)

3.4.1 Hydro dynamic coefficients

The most commonly used quantity for describing the damping in a system is the damping ratio ξ, which shows the relationship between the damping and critical damping (Larsen, 2012).

$$\xi = \frac{B}{B_{cr}} \tag{3.55}$$

Were critical damping B_{cr} depends on the restoring C and the mass M, defined by Equation 3.56

$$B_{cr} = 2\sqrt{M4C_4} \tag{3.56}$$

Damped natural frequency for a structure when the damping ratio is ξ<1, is sub-critical damping and is the most common case for offshore structures. The damped natural frequency ω_d

$$\omega_d = \omega_0\sqrt{1-\xi^2} \tag{3.57}$$

(Chakrabarti, 2005) Where the natural period T_n is given in Equation 3.58

$$T_n = 2\pi\sqrt{\frac{(M+A)}{C}} \tag{3.58}$$

Where the mass M is presented in the mass matrix in Table 3.1. When computing the natural period in the oscillatory angular motions as roll, pitch and yaw we express the mass as moment of inertia I as shown in Equation 3.59

$$I = Mr^2 \tag{3.59}$$

Where r is the radius of gyration. The mass matrix is presented in Table 3.1

Table 3.1: Mass matrix

	1	2	3	4	5	6
1	M	0	0	0	Mz_G	0
2	0	M	0	-Mz_G	0	0
3	0		M	0	0	0
4	0	-Mz_G		I_4	0	-I_{46}
5	Mz_G	0	0	0	I_5	0
6	0	0	0	-I_{46}	0	I_6

Where M is the mass of the vessel and I is the mass moment.

For roll motion we may express the restoring moment C_{44} from Equation 3.58 as follows

$$C_{44} = \rho g \nabla G M_T \tag{3.60}$$

The critical quadratic damping b2 used in WADAM is obtained from Equation 3.61.

$$b_2 = \frac{B_2}{2C_4 \frac{180}{\pi}} \tag{3.61}$$

Where B_2 is the estimated quadratic damping, this value is usually obtained by performing a free decay test.

3.5 Fatigue

Fatigue occurs when the structure is subjected to an alternating loading. If the loading cycles continues cracks may develop in the steel, and lead to reduced strength, known as fatigue. The material strength is not reduced from fatigue, but the developed cracks on the other hand will reduce the strength of the structure. Especially stresses in the welds are critical when it comes to fatigue lifetime.

Relative fatigue damage during 3 hour-duration sea state is described by fatigue measure denoted in Equation 3.62.

$$F_m(H_s, T, \theta) = \frac{a^m}{T[ln(10800/T)]^{m/2}} \tag{3.62}$$

Where $F_m(H_s, T, \theta)$ is the fatigue measure, m is the slop of the S-N curve, and a is the acceleration.
It describes how much the roll motion contributes to fatigue damage during one sea state. To obtain the total fatigue damage during a voyage, we need to apply this equation for each sea state that the barge is exposed to on the voyage. The total fatigue damage is described by a weighed fatigue formulation found in Equation 3.63, where the probability of duration of each sea sate is taken into account.

$$F_{weigt} = \sum_{H_s, T_p, \theta} F_m(h_s, t_p, \theta) \times p(h_s, t_p, \theta) \times T \tag{3.63}$$

Where $p(h_s, t_p, \theta)$ is the probability of the occurrence for a sea state.

Fatigue damage on the cargo is mainly due to inertia forces, and the fatigue stress is linearly proportional to the acceleration at COG (Yang *et al.* , 2018).

Chapter 4

Analysis setup

In this chapter a brief description of the softwares used in this thesis will be presented, and how they are used to solve the current problem. Furthermore a description of the model will be included.

4.1 Softwares

The softwares used is GeniE to create the model, HydroD/WADAM to perform the analysis, Postresp to print out the RAOs, and MATLAB to calculate for the post processing and plotting.

4.1.1 GeniE

GeniE is a design and analyzing tool as part of the Sesam suite from DNV GL. It is used for modeling and analyzing offshore structure consisting of beams and plates. GeniE covers the entire lifecycle of a marine structure from the initial design phase with structural analysis, through the final design, and re-design if the structure needs repair or modifications. It is one of the few analyzing tools where modeling, FEA (Finite Element Analysis) and Postresp (result processing) can be performed in the same Graphical User Interface (GUI) with one single model (DNV-Software, 2014).

GeniE is used to create a panel model of the barge, since the analysis requires a different software. The barge is modeled by first creating the geometry and

then adding a mesh. A detailed panel model provided by DNV GL is used for the calculations in HydroD/WADAM.

4.1.2 HydroD/WADAM

HydroD and WADAM are also part of the Sesam platform. HydroD's main purpose is hydrostatic and stability analysis. However it is also used as GUI for WADAM and WASIM, Which is more relevant for this problem.

Wave loads and motions are computed in FD by WADAM. WADAM is an analysis program for calculation of wave interacting with structures for fixed and floating structures. In this case we are looking at a ship hull and want to calculate hydrostatic data and global responses. WADAM calculates loads using potential theory described in Section 3.2.2

The panel model is read by WADAM from the input file T^*.FEM generated in GeniE. When the response analysis is completed, the results is stored in a G-file and is ready to be used in the statistical post processing in Postresp. The G-file is also used in SIMA for the TD analysis, where the hydrodynamic data, including potential damping from potential theory is implemented. (DNV-Software, 2008).

4.1.3 Postresp

Postresp is used for statistical post processing and viewing/printing of transfer functions generated by WADAM. First of all we can plot the response variable (RAO) which is compared with the response variable obtained in TD. This is valid only for regular waves. For the irregular waves we need to compare the response spectra. This is done by defining a sea state, in this case a JONSWAP spectrum, and then creating a response spectrum. The results from Postresp are copied into a text document and imported into MATLAB which is used for the rest of the post processing.

4.2 Description of the model

In this section we will define the model and describe the procedure of calculating the global response in WADAM. First of all, we assume no forward speed. The purpose of this analysis is to obtain the motion components on the barge

based on the global responses, and create a response spectrum that later will be compared with the response spectrum from TD.

First step is to define the sea state and environmental data. The sea state is defined by wave frequency components and wave headings. For the irregular case we also define a wave spectrum to obtain the linearized damping coefficients. The environmental data contains gravity, air and water density, air and water kinematic viscosity and water depth. Furthermore we include the panel model from GeniE and define the mass model and coordinate system. Since roll damping is our main focus we include bilge keels to get the roll damping as accurate as possible. The additional linear and quadratic damping obtained from a decay test is also included. The quadratic damping is included as a fraction of critical damping.

4.2.1 Initial data

From DNV GL we got some initial data on the barge-cargo system, where the main dimensions of the barge is presented in Table 4.1

Table 4.1: Initial data

Length [m]	267
Width [m]	71
Draught at FPP [m]	7.8
Draught at APP [m]	7.8
Weight [t]	119662
GM4 [m]	26.94
LCG from APP [m]	133.789
TCG from center line to port side[m]	-0.001
VCG from base line of the vessel [m]	30.807
Radius of Gyration of Roll	33.58

Where GM4 is the metacentric height, APP is after perpendicular, FPP is the forward perpendicular, LCG is the longitudinal center of gravity, TCG is the transverse center of gravity and VCG is the vertical center of gravity.

4.2.2 Mass model

A mass model is required in WADAM for both the hydrostatic calculations and in the equation of motion. The global mass matrix is specified in Table 4.1 provided by DNV GL. This includes the total mass of the structure including the jacket, center of gravity and the gyration of radii. The center of gravity is specified with respect to the input coordinate system, while the gyration of radii is with respect to the global coordinate system (DNVGL-Software, 2017).

The mass model is modeled as transverse beams representing the mass of each section, and may be defined in two different ways; a 6x6 mass matrix or user defined mass parameters as done in this case.

4.2.3 The panel model

For calculation of the hydrodynamic loads a panel model of the barge created in GeniE is used. It describes the wet surface of the model and has symmetry in the XY-plane. This is to reduce the computational time and use of CPU and disc space.

The panel model is imported to HydroD, and the origin is changed to x = COG, y = at the center line and Z is at the water line. Only half of the model is given, and has symmetry in XZ-plane. It must be symmetrical for HydroD to be able to calculate the viscous roll damping. The model is only design for the geometry below the water line, the rest of it is described by the mass model.

The hydro static analysis was not possible to execute with the provided model from DNV GL. The model is a panel model describing the barge below the water surface, along with a mass model describing the weight distribution for the complete ship with cargo. Data from the hydrostatic analysis is therefor provided by DNV GL, and includes the GZ-curve. The dynamic analysis on the other hand is possible when the initial data from the hydro static analysis is known.

The output result file from WADAM is a .LIS file. Most of the results from the WADAM analysis are non-dimensional and needs to be dimensionalized. This can be done by using dimensionalizing factors found in the WADAM user manual (DNVGL-Software, 2017). Alternatively we can use Postresp to analyze the final results. If so, we do not need to dimensionalize the results, and it is

possible to visualize the results.

The barge is divided into 3 parts, mid-ship, bow and stern areas. Since the barge has more curves and details in the bow and stern the mesh size is slightly finer compared to the mid-ship. The mesh consists of quadrilateral elements on 4x1 meters in the mid-ship and 1.2x1 in the bow and stern. This gives a mesh composed by 4800 panels in the model. An illustration of the model in GeniE with the mesh is shown in figure 4.1

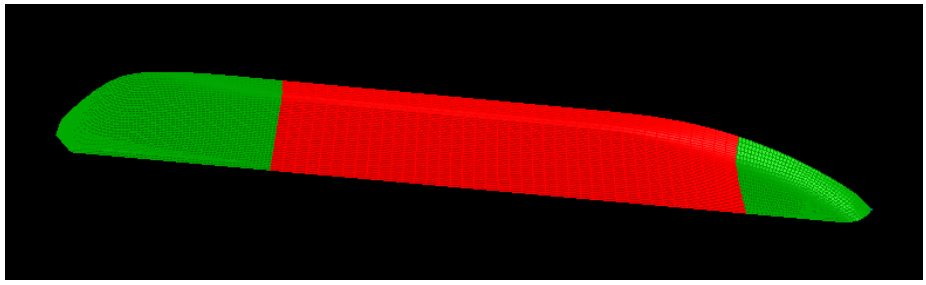

Figure 4.1: Mesh from GeniE

Where we can see half of the barge model divided into three mesh sections.

4.2.4 GZ-curve

The GZ-curve describes the stability of the vessel, and is obtained by a static stability analysis. Due to the limitations in the model discussed in the previous section, the GZ-curve is provided by DNV GL shown in Figure 4.2.

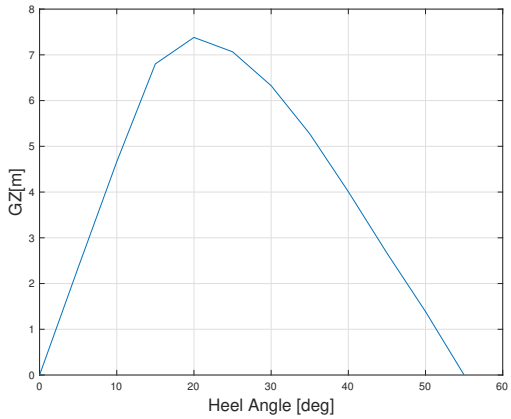

Figure 4.2: GZ-curve

Where GZ is the righting lever of the vessel. We need the GZ-curve when we want to include bilge keels.

4.2.5 Bilge keel

The purpose of a bilge keel is described in Section 2.2.3. When including a bilge keel there are two things that needs to be defined; the dimensions and location of the bilge keel, and strips to be able to calculate the damping in WADAM. The basic data of the bilge keel is presented in Table 4.2.

Table 4.2: Bilge keel

Length [m]	102.5
Width [m]	0.8
Angle [deg]	-45.9
Bilge radius [m]	2
Z pos. from vessel bottom [m]	0.56
Y pos. from center line [m]	34.43
X pos. from APP [m]	79 to 181.5
Number of strips	17
Strip spacing [m]	10

The bilge keel is 0.56m above the vessel bottom and 34.43 m away from the

center line in transverse direction. In longitudinal direction, it starts from 79 m, and ends at 181.5 m with APP as reference. The bilge keel angle is -45.9 deg corresponding to a coordinate system with the xy-plane coincide with the still water plane.

To calculate the damping from the bilge keel we divide the bilge keel section of the barge in a finite number of strip. The strip model has to defined in the longitudinal direction which will be used to estimate the viscous damping. A length of 10 m is used for this case. Tanaka/Kato roll damping model used in this viscous damping analysis. An illustration of the model in WADAM is shown in Figure 4.3. Where we can see the strips in purple at the mid-ship.

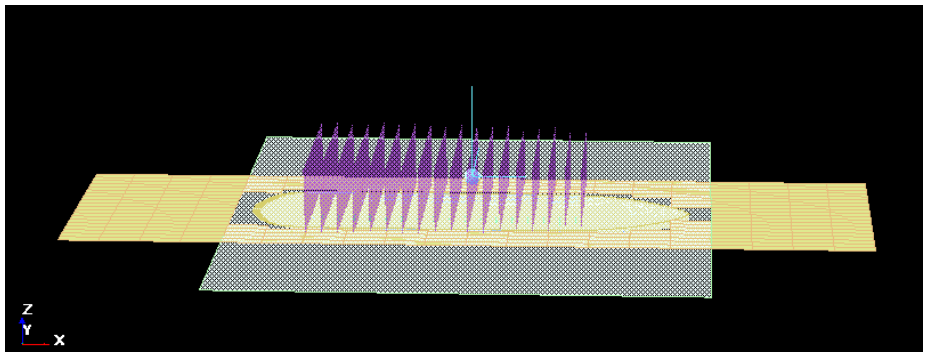

Figure 4.3: Model from WADAM

4.2.6 Procedure

The objective is divided into two main cases, analyses with regular waves and analyses with irregular waves. Where linearization of the roll damping is the main focus for both cases. For the regular waves there is no need for a sea state, and with no sea state it is not possible to the stochastic linearization by using WADAM. This means that it must be done manually, by iteration of Equation 3.44. The quadratic damping from the decay test and the eigenfrequency is kept constant. The RAO and equivalent damping are dependent on each other, hence we must iterate. Starting with only the linear damping and calculating the maximum response, this gives a new equivalent linear damping. Further we do a new analysis with the new equivalent damping, and do this un-

til the results are converging. More on equivalent linearization on in Section 5.2.

When it comes to the case with irregular waves, WADAM takes care of the stochastic linearization. First of all, we define a sea sate, the linearized quadratic damping will be different for each sea state. The sea state has a duration of 3 hours, thus we avoid effects from the transient phase in the beginning of the analysis. Furthermore, we include the fraction of critical quadratic damping defined as 0.0091, and then we define the convergence criteria which is set to 0.1 %. The convergence criteria is based on the error of the standard deviation of the response spectrum $S(\omega)$ from two consecutive iterations. The standard deviation σ can be found by the square root of the variance σ^2 obtained by Equation 3.53. The iteration procedure is shown in Figure 4.4.

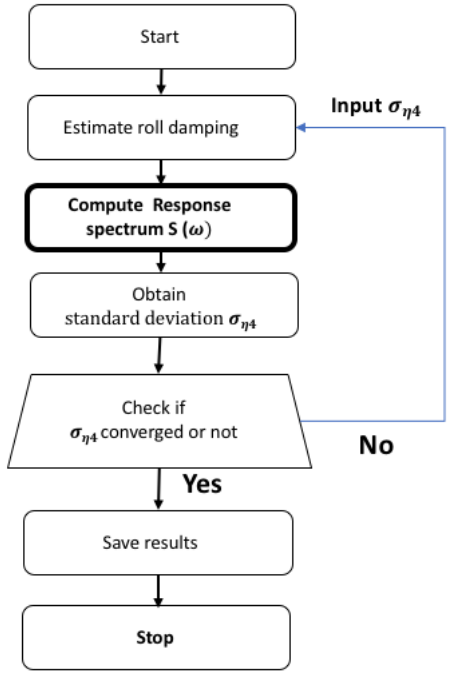

Figure 4.4: Iteration procedure

Chapter 5

Results

In this section, the results obtained throughout this thesis will be presented and discussed. First of all the basic hydrodynamic results from TD and FD will be presented and compared. Furthermore, we have the results from analyses with regular and irregular waves, which will be compared with the results in TD. Since the results are not exactly the same from the TD and FD analysis, we will go through potential errors that caused the differences.

Basic input used in the analysis is presented in Table 5.1

Table 5.1: Basic input

Parameter	Value	Unit
Linear damping B_1	3.92e9	[Nms]
Quadratic damping B_2	2.17e11	$[Nms^2]$
Fraction of critical damping b_1	0.024	[-]
Fraction of critical damping b_2	0.0091	[1/deg]
Stiffness	3.21e10	[Nm]
Total roll inertia	2.08e11	$[Kgm^2]$

Where b_1 is the fraction of critical linear damping as shown in Equation 3.55 and b_2 is the fraction of critical quadratic damping shown in Equation 3.61.

5.1 Basic hydrodynamic results

In this section, basic hydrodynamic results from TD and FD will be presented and compared. First of all the natural periods, then mass, restoring and potential damping matrices will be presented. There will also be a comparison of the excitation moment in roll motion for both 45 and 90 degrees wave direction.

Natural periods for heave, roll, and pitch motion are presented in the Table 5.2. The natural periods are dependent on the added mass, which is dependent on the wave period T. Thus, the natural period varies as a function of wave periods. In the table below a wave period of 16s is used in FD. In TD decay tests are performed to obtain the natural periods.

Table 5.2: Natural period

	FD [s]	TD [s]
Heave	12.1	11.7
Roll	15.6	14.8
Pitch	11.5	10.7

In FD the natural period is 0 for surge, sway and yaw due to zero restoring, we can easily see this by applying equation 3.58 Where M is found in the mass matrix in Table 5.3and C in the restoring matrix 5.4. In SIMA for the TD analysis on the other hand, stiffness is added in surge, sway and yaw to obtain the natural periods.

From the mass matrix 3.1 in Section 3.4.1 we can obtain the Mass matrix for this case shown in the following table.

Table 5.3: Mass matrix

	1	2	3	4	5	6
1	1.197e8	0	0	0	2.753e9	-1.197e5
2		1.197e8	0	-2.753e9	0	0
3			1.197e8	-1.197e5	0	0
4				1.983e11	0	0
5					4.914e11	2.753e6
6						4.181e11

As we can see from Table 5.3 the mass input given in hydroD is the same in all translations and in the rotations we need to multiply by r^2, shown in Equation 3.59. M_{34} and I_{56} is not suppose to be there, it could be due to some errors in the calculations by WADAM. Since they are small compared to the rest of the results, we can set them to 0.

In Table 5.4 we have the restoring matrix.

Table 5.4: Restoring matrix

	1	2	3	4	5	6
1	0	0	0	0	0	0
2		0	0	0	0	0
3			1.716e8	0	1.372e9	0
4				3.178e10	0	-6.523e8
5					8.668e11	-1.173e6
6						0

As we can see from the table there is no restoring in surge, sway and yaw.

Total damping is the sum of potential damping and viscous drag from Morison's theory. The potential damping matrix is frequency dependent, and is therefor shown in Table 5.5 for a period of 16s.

Table 5.5: Potential damping matrix

	1	2	3	4	5	6
1	8.798e5	0	6.23e4	0	6.142e6	0
2		5.247e6	0	-1.978e8	0	8.164e6
3			1.57e8	0	1.362e9	0
4				7.545e9	0	3.455e8
5					4.469e11	0
6						4.977e9

The matrices above are only shown for one side of the diagonal, this is due to symmetry. For the potential damping there are some minor differences, but we assume symmetry.

The excitation force is also an important part of the equation of motion. Excitation moment in roll for 45 and 90 degrees is shown in Figure 5.1.

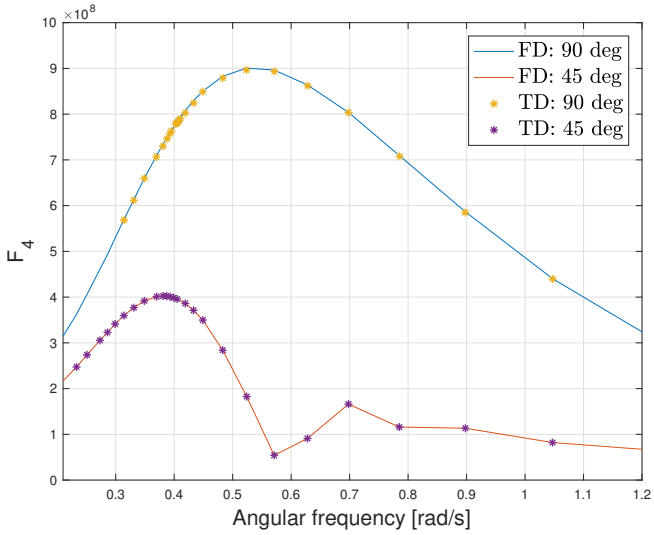

Figure 5.1: Moment in roll - 90 vs 45 deg

The excitation force will not change if we add quadratic damping, response on the other hand is dependent on the damping. There is no surprise that the excitation force is the same in TD and FD, since the excitation force is imported from the FD analysis in WADAM, to SIMA for the TD analysis.

A comparison of the response with linear damping for wave heading 0, 15, 45 and 90 degrees is presented in Figure 5.2.

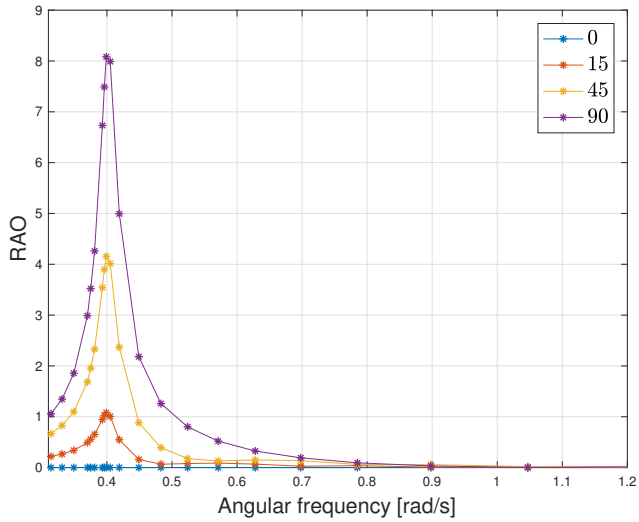

Figure 5.2: Comparison of RAO: 0, 15, 45 and 90 degrees

From the figure above, we can see that there is no response in roll motion when there is waves coming straight towards the bow, and the maximum response occurs when we have beam sea. The dots in the plot are the frequency components used in the analysis. To get more accurate results we can add more frequency components, but then the computational time will increase.

5.2 Regular waves

In this section, we consider regular waves with wave amplitude of 1m and wave directions of 45 and 90 degrees. The goal here is to do a equivalent linearization of the quadratic roll damping provided by DNV GL and obtain the roll motion RAO. The results from the FD analysis are compared with the TD analysis. The comparison is done in order to verify that the model in FD and TD is comparable. Since we are using regular waves, we can not use the build in stochastic linearization option in WADAM, hence the iteration is done manually. Equation 3.44 is used for this purpose where the linearized damping B_{eq} and the max response $\eta_{4,max}$ is changed for each iteration, while the eigenfrequency is kept constant. The convergence test is shown in Figure 5.3, where $\eta_{4,max}$ is the value converging.

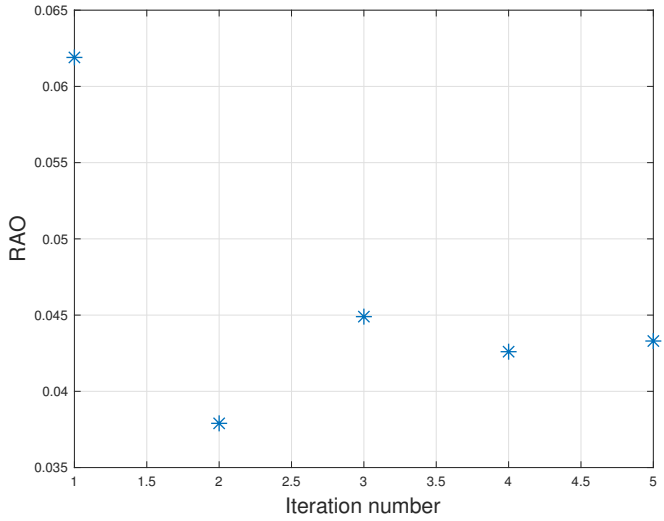

Figure 5.3: Convergence test of the equivalent linear damping

Where the start value of linearized quadratic damping is set to 0. All inputs to WADAM are given by the additional linear damping and the linearized quadratic damping. The problem with doing this process manually is that it is very time-consuming. This is the equivalent linear damping for one sea state with an amplitude equal to 1m and 45-degree wave direction. The process must be repeated for all the wave heights, periods and wave directions that are of interest.

5.2.1 Comparison of linear damping

In this section, the response in regular waves and with linear damping will be presented for all DoF's in 45 and 90 [deg] wave direction. This part of the analysis is performed to see if the model in TD is the same as the FD model. The basic hydrodynamic data is computed in WADAM and then imported into SIMA for the TD analysis, which means the results should be similar. If they are similar in the reality will be investigated in this section. In TD, the barge is given stiffness in surge, sway and yaw to give the vessel eigenperiods. SIMA's main purpose is moored systems and not free floating systems like the barge. This is why we need to implement stiffness in the TD analysis. It is important to pay attention to the motions coupled to roll motion; sway and yaw, as they

can give a significant contribution to the roll motion.

In Figure 5.4a and 5.4b, the comparison of FD and TD for response in heave with 45 and 90-degree wave headings is presented.

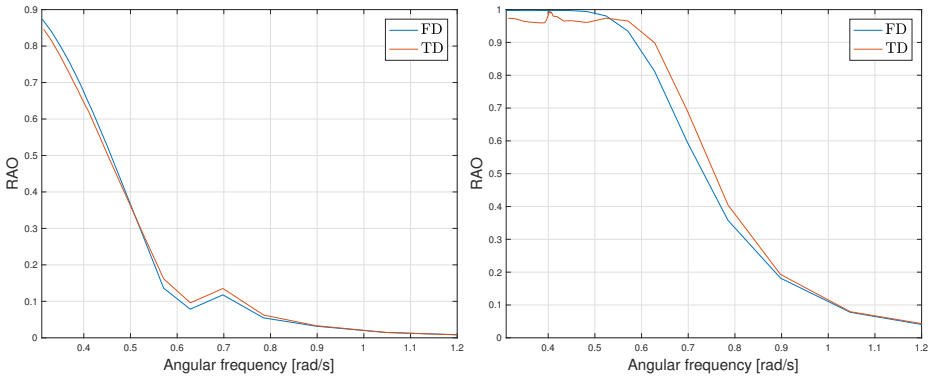

(a) Heave 45 [deg]

(b) Heave 90 [deg]

Figure 5.4: Linear damping in regular waves: Heave

As we can see from Figure 5.4a and 5.4b, the response is almost identical in TD and FD for heave. When the wave frequency is low, the heave response follows the wave elevation, this why the response in the figure goes towards 1 for higher wave frequencies.

Surge is one of the coupled motions to roll motion, hence we must look for any deviations in response. The response for surge motion is presented in Figure 5.5a and 5.5b.

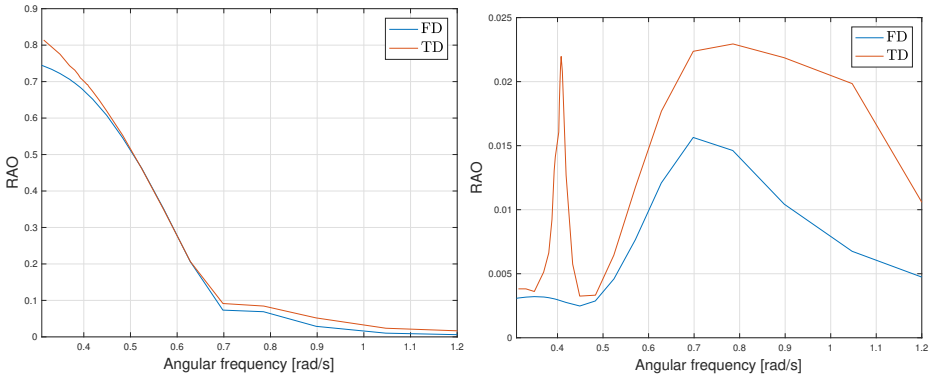

(a) Surge 45 [deg]

(b) Surge 90 [deg]

Figure 5.5: Linear damping in regular waves: Surge

If we are considering head sea, the vessel response will go towards 1 for low wave frequencies, similar to heave motion. We can se the tendency in Figure 5.5a. In Figure 5.5b, the motion response is very small, this is due to the wave direction. When we have beam waves there is almost no response in surge direction, they are perpendicular to each other. The large peak at $\omega = 0.4$ is most likely due to a coupling effect from the roll motion. This is where roll motion has its eigenfrequency.

The results in pitch motion are also fairly similar in both the TD and FD analysis, as shown in Figure 5.6a and 5.6b.

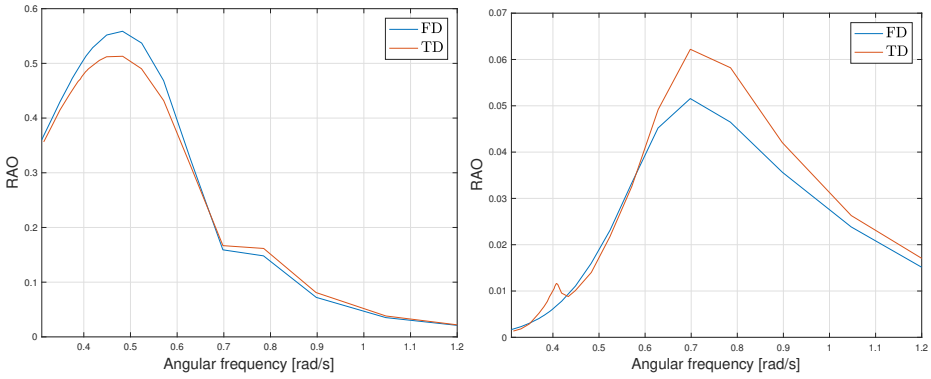

(a) Pitch 45 [deg]

(b) Pitch 90 [deg]

Figure 5.6: Linear damping in regular waves: Pitch

In Figure 5.7a and 5.7b, the response for sway motion is presented. Sway was the most problematic motion to get correct. We stared with a stiffness value in sway that gave very similar results for sway response in TD and FD, but this stiffness value gave to much contribution to the roll motion. In FD there is no stiffness, also known as restoring, in sway motion.

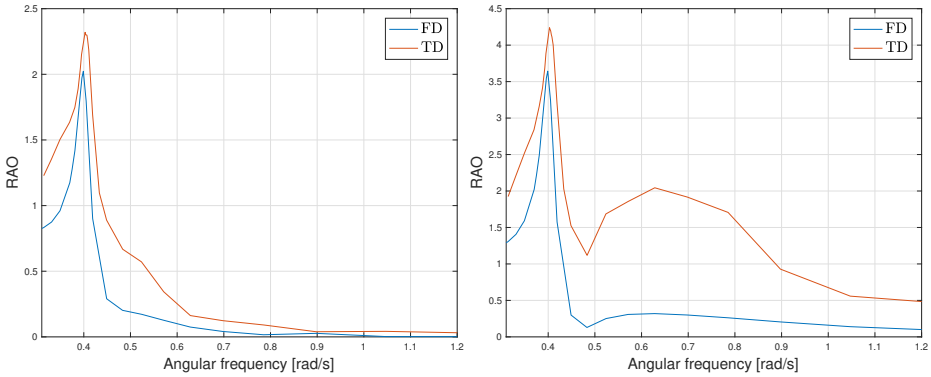

(a) Sway 45 [deg] (b) Sway 90 [deg]

Figure 5.7: Linear damping in regular waves: Sway

The response results in sway is pretty good, but the difference here is necessary to get good results in roll motion. This is due to the coupling effects between them. In both cases, 45 and 90 degrees, the peak is located at the roll eigenfrequency.

Roll motion is the most interesting DoF for the purpose of this thesis. The roll motion response is shown in Figure 5.8a and 5.8b.

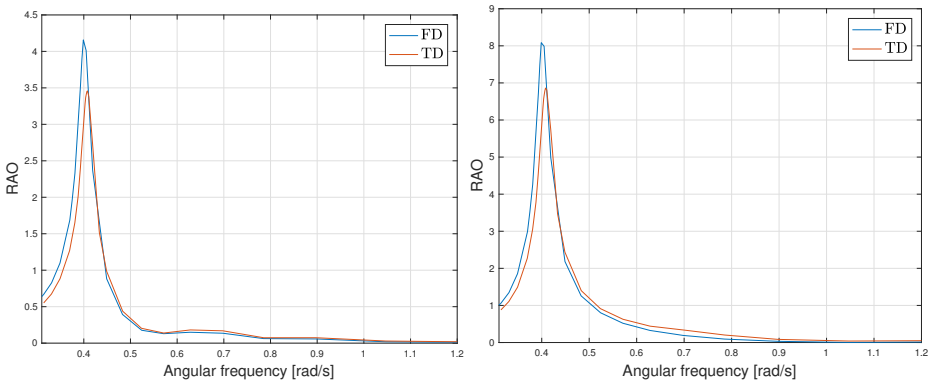

(a) Roll 45 [deg]

(b) Roll 90 [deg]

Figure 5.8: Linear damping in regular waves: Roll

The roll motion response variable has almost the same shape for both 45 and 90 degrees, but there are some minor differences in the results from the TD and FD analysis. The damping in the TD analysis is larger in the TD model compared to the FD model, which gives a smaller response in TD. This could be due to coupled effects from sway and yaw. More on that in Section 5.4. The natural frequency is around 0.4 [rad/s] for both cases, which is really important when comparing the FD and TD results.

Yaw is also one of the coupled motions to the roll motion, presented in Figure 5.9a and 5.9b.

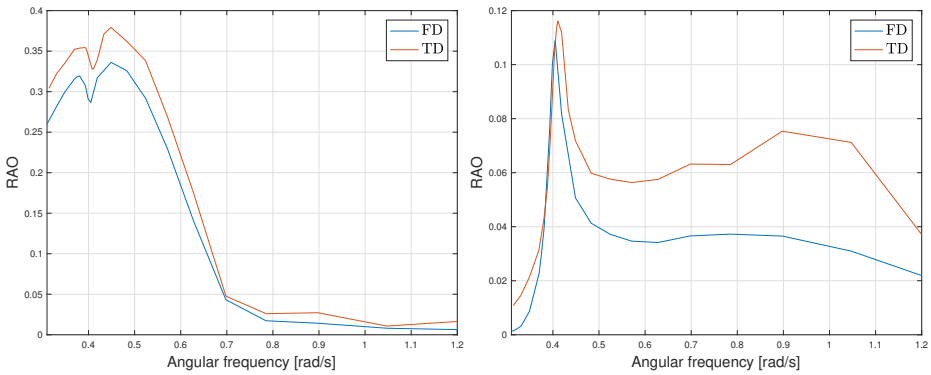

(a) Yaw 45 [deg]

(b) Yaw 90 [deg]

Figure 5.9: Linear damping in regular waves: Yaw

In Figure 5.9a, there is a negative peak at the eigenfrequency for roll, this indicates coupling between the two motions. In Figure 5.9b the peak is almost at the eigenfrequency in roll motion, which is natural when we are considering beam waves.

5.2.2 Comparison of linearized quadratic damping

In this section the equivalent linear damping is used as input. The method for obtaining this equivalent damping is described in Section 5.2. Only results from 45 degrees wave heading is presented in this section to show how to linearize the damping manually. In general the plots with linearized damping have pretty much the same shape as for only linear damping, but the response is smaller due to the increased damping.

We can expect the results in heave, surge and pitch to be almost identical before and after the quadratic damping is included. This is because there are no coupling effects between the them and roll motion. Response in heave and pitch is presented in Figure 5.10a and 5.10b respectively.

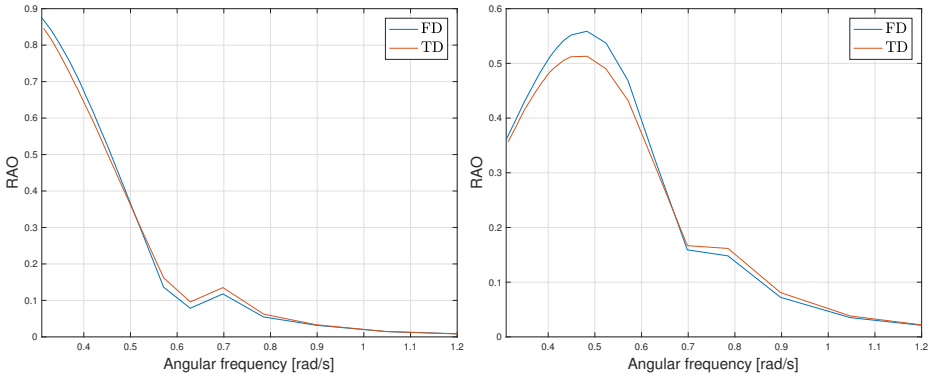

(a) Heave 45 [deg] (b) Pitch 45 [deg]

Figure 5.10: Linearized quadratic damping: Heave and Pitch

The plots of heave and pitch confirm the hypothesis of no influence on the response when increasing the roll damping.

Response in surge and roll is presented in Figure 5.11a and 5.11b respectively. We expect to see no difference in surge, of the same reasons as for heave and pitch. Roll motion response on the other hand will definitely change due to the increased damping.

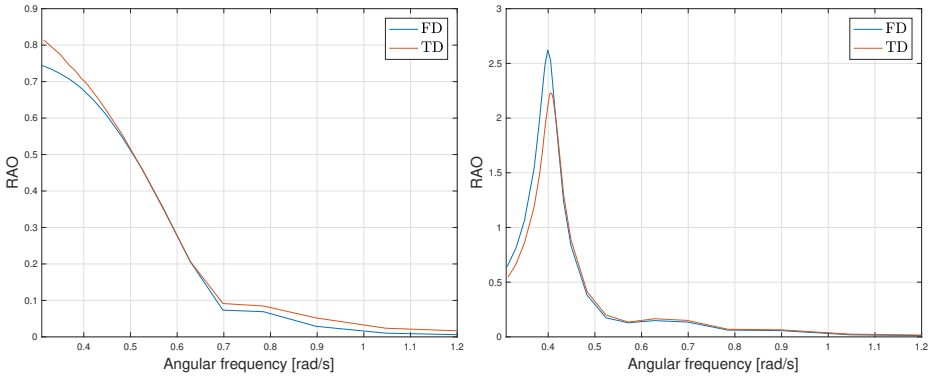

(a) Surge 45 [deg]

(b) Roll 45 [deg]

Figure 5.11: Linearized quadratic damping: Surge and Roll

As expected, the surge motion is the same as for the linear damping. For roll motion the RAO was about 4.1 with only linear damping, while for the case with linearized quadratic damping the RAO is 2.6, both results from the FD analysis. This shows that including the quadratic damping for this particular sea state, the response is reduced by about 37%. In Figure 5.12, the effect of quadratic damping is illustrated.

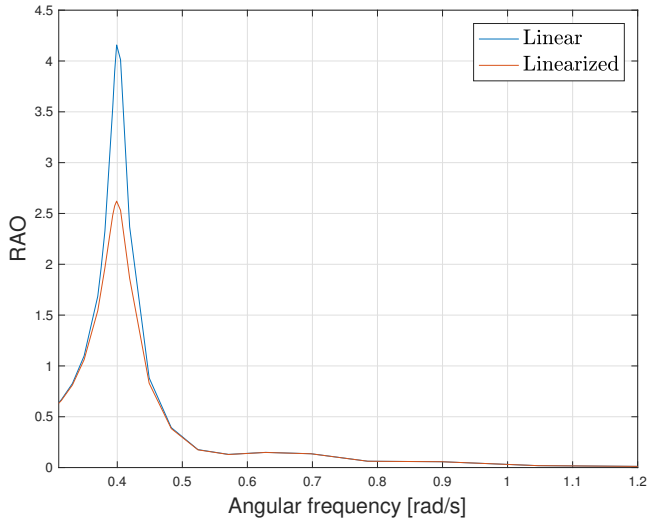

Figure 5.12: Roll motion: Linear vs. linearized quadratic damping

Yaw and sway are both coupled to roll motion and we expect to see a decrease in response, they are presented in Figure 5.13a and 5.13b respectively.

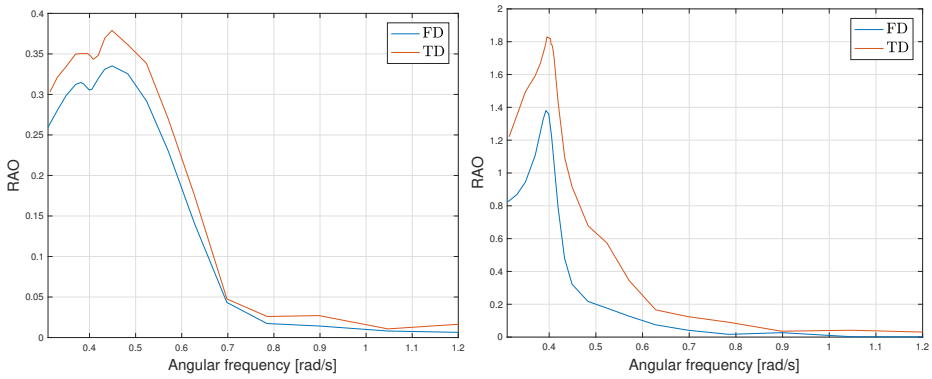

(a) Yaw 45 [deg]

(b) Sway 45 [deg]

Figure 5.13: Linearized quadratic damping: Yaw and Sway

If we compare the results in yaw shown in Figure 5.13a, with the results from the linear damping analysis, we can see that they are pretty similar. We expected them to be different due to the coupling, but this shows that the coupling effect is low in this case. Sway motion on the other hand is significantly reduced compared to the analysis with linear damping, which means that it is coupled to the roll motion, as we expected.

The linearized quadratic damping term is compared with the quadratic damping in SIMA, shown in Figure 5.14.

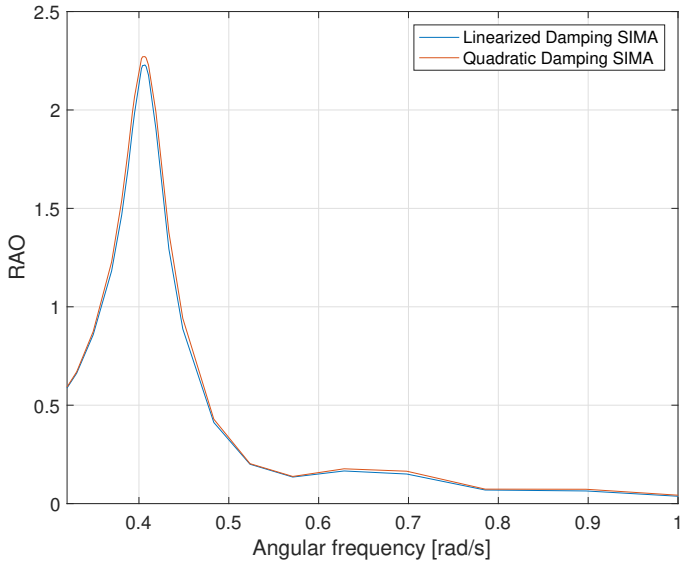

Figure 5.14: Qudratic vs Linearized damping computed in SIMA

This shows that the manual linearization is very precise for regular waves.

5.3 Irregular waves

Now that we have verified that the models in SIMA and WADAM are pretty similar by the analysis in regular wave condition, we can move over to irregular waves. we are going to use the stochastic linearization method to obtain the equivalent linearized roll damping. Since the waves are changing within a sea

state, we need to look at the response spectrum to compare the results. The response spectrum is given by Equation 3.33.

The irregular wave cases investigated in this section are presented in Table 5.6. All the other sea states are represented in Appendix 6.4.

Table 5.6: Sea states

Hs [m]	1.5	2.5	3.5	4.5	5.5	6.5
Tp[s]	7.5	8.5	9.5	10.5	11.5	12.5

The response spectrum is calculated based on JONSWAP spectra with spectrum variables from Table 5.6. The goal of this investigation is to compare the response spectrum computed in TD and FD, to see if the linearization is good. Analyses with both quadratic damping and linearized damping will be performed in TD and compared with the results from the FD analysis.

The linearized quadratic damping for each sea state is presented in Table 5.7 for 45 degrees wave heading and Table 5.7 for 90 degrees wave heading.

Table 5.7: Stochastic linearized damping - 45 deg

Hs/Ts	7.5	8.5	9.5	10.5	11.5	12.5
1.5	1.06E+08	1.43E+08	1.89E+08	2.81E+08	4.38E+08	6.29E+08
2.5	1.77E+08	2.39E+08	3.14E+08	4.64E+08	7.16E+08	1.02E+09
3.5	2.48E+08	3.34E+08	4.39E+08	6.44E+08	9.85E+08	1.39E+09
4.5	3.18E+08	4.30E+08	5.67E+08	8.30E+08	1.26E+09	1.77E+09
5.5	3.86E+08	5.19E+08	6.85E+08	1.01E+09	1.52E+09	2.11E+09
6.5	4.60E+08	6.13E+08	8.09E+08	1.18E+09	1.77E+09	2.45E+09

Table 5.8: Stochastic linearized damping - 90 deg

Hs/Ts	7.5	8.5	9.5	10.5	11.5	12.5
1.5	1.50E+08	2.67E+08	4.41E+08	7.03E+08	1.03E+09	1.39E+09
2.5	2.51E+08	4.45E+08	7.32E+08	1.16E+09	1.68E+09	2.22E+09
3.5	3.51E+08	6.23E+08	1.02E+09	1.60E+09	2.29E+09	3.01E+09
4.5	4.51E+08	8.00E+08	1.31E+09	2.04E+09	2.89E+09	3.74E+09
5.5	5.49E+08	9.71E+08	1.59E+09	2.46E+09	3.45E+09	4.44E+09
6.5	6.52E+08	1.15E+09	1.87E+09	2.87E+09	4.01E+09	5.12E+09

Where the linear damping has unit [Nms]. To obtain the stochastic linearized damping coefficients it required between 3 and 9 iteration.

To visualize the quadratic damping contribution, the results from the stochastic linearization from Table 5.7 and 5.8 are presented as surface plots shown in Figure 5.15 and 5.16 respectively.

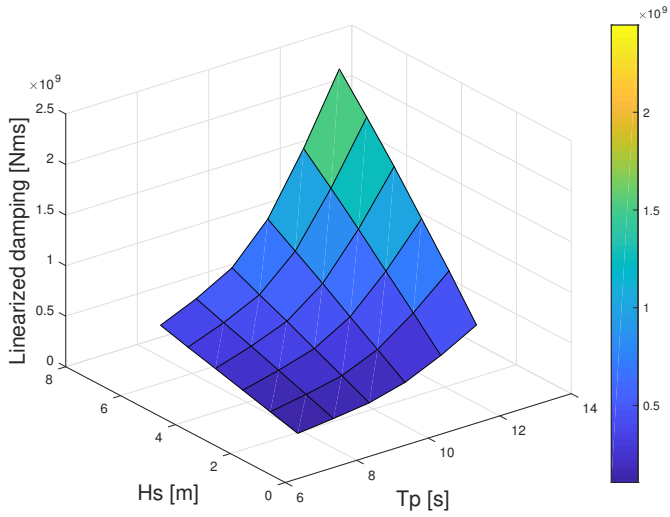

Figure 5.15: Stochastic linearized damping - 45 deg

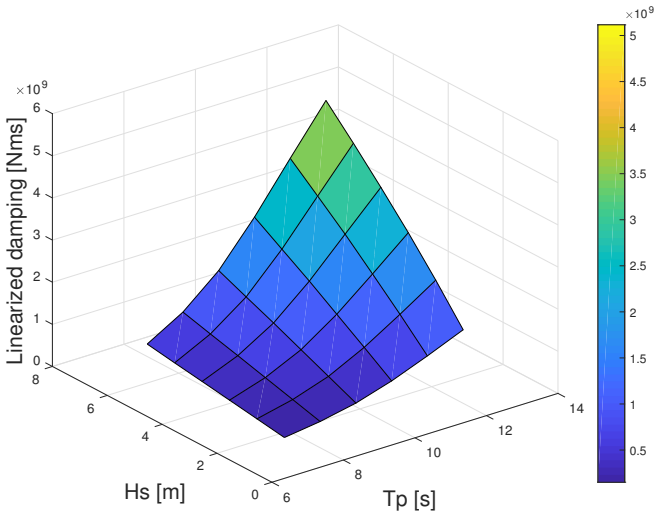

Figure 5.16: Stochastic linearized damping - 90 deg

As indicated in the plots, the linearized damping varies non-linearly with the sea state, exactly as expected, since we are dealing with quadratic damping. It is important to be aware of the damping varies non-linear with the wave period Tp, and linear with the hight Hs. When it comes to the difference in damping for 45 and 90 degrees wave heading, we can see that there is more than two times as much damping in the case with 90 degrees wave heading.

5.3.1 Response spectrum: Hs = 4.5 [m] and wave direction = 45 [deg]

In this section some selected response spectra are presented. The selected spectra have a significant wave height Hs = 4.5 meters, and a wave direction of 45 degrees. All periods are represented to get a good picture of how the wave spectrum evolves with increased period.

In Figure 5.17a and 5.17b we have a sea sate with peak-periods equal to 7.5s and 8.5s respectively.

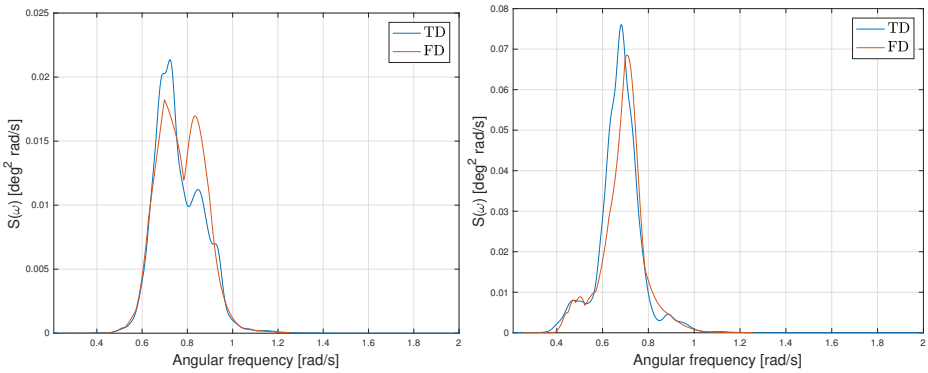

(a) Tp=7.5s, 45deg (b) Tp=8.5s, 45deg

Figure 5.17: Response spectrum comparison

At this small periods, the wave frequency is to high to give any significant response. In Figure 5.17a there is two peaks, the one to the right is at the wave peak-frequency and the one to the left is due to an eigenfrequency. There is not much difference between the response spectrum computed in FD and TD, since the response is small, but we can see a slightly larger response at the wave peak-frequency computed in FD. In Figure 5.17b there is only one significant peak, located at the wave peak-frequency. However, we can see that there is a small response peak evolving at the eigenfrequency for roll motion.

Response spectra for the periods 9.5s and 10.5s is presented in Figure 5.18a and 5.18b respectively.

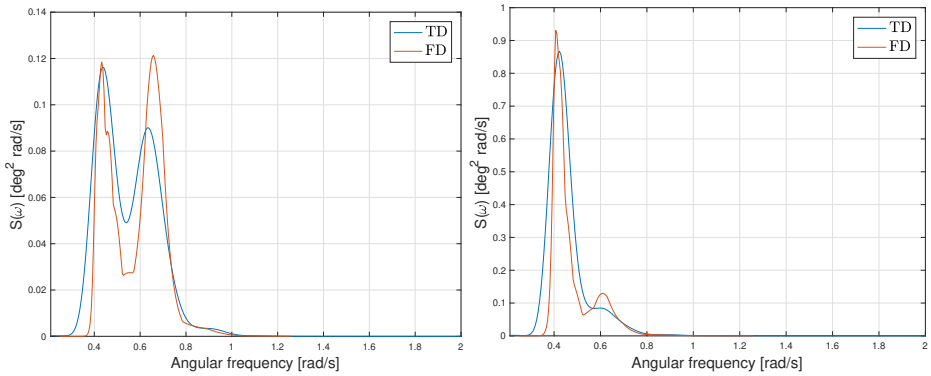

(a) Tp=9.5s, 45deg (b) Tp=10.5s, 45deg

Figure 5.18: Response spectrum comparison

In Figure 5.18a we see that the response is equally affected by the roll motion eigenfrequency and the wave peak-frequency. The wave peak period is still too small to give a significant response. When it comes to Figure 5.18b the response is significantly bigger, almost 10 times as big compared to Tp=9.5s.

Figure 5.18a and 5.18b represents the response spectrum for the highest periods considered in this analysis, with a wave peak-period of 11.5s and 12.5s respectively.

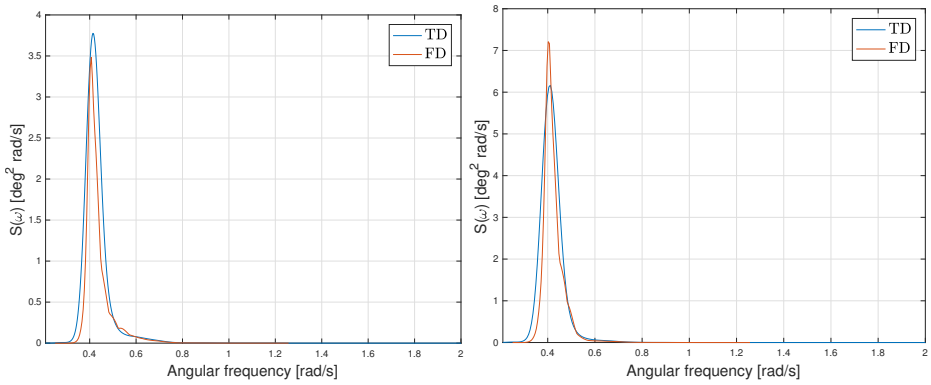

(a) Tp=11.5s, 45deg (b) Tp=12.5s, 45deg

Figure 5.19: Response spectrum comparison

The response for this two sea states are much bigger than the other sea states considered in this analysis. Both the response spectra coincide with the eigen-frequency in roll motion.

Regarding the difference between the FD and TD analysis, we can see a clear difference in the energy amount for the case with Tp = 11.5s. The response spectrum obtained in the FD analysis has a lower peak and is narrower. The case with Tp = 11.5s, is the case with the largest error, even though the two graphs look very similar. In the case with Tp = 12.5 shown in Figure 5.18b, the peak response obtained in the FD analysis is larger, but the spectrum is narrower. This gives a more equal energy amount for the FD and TD analysis than for Tp = 11.5.

An illustration of the relationship between the response variable, wave spectrum, and the response spectrum is shown in Figure 5.20.

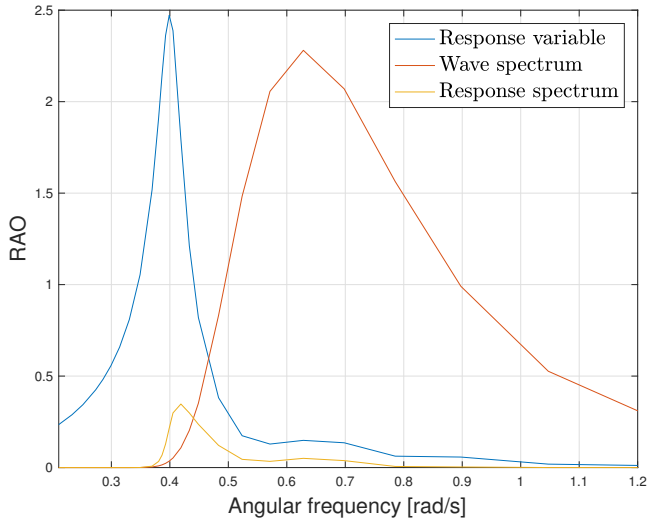

Figure 5.20: RAO, Wave spectrum and Response

Here we have an eigenfrequency of 0.4 [rad/s], and a wave peak-frequency of 0.63 [rad/s]. The closer these two frequencies are, the larger response we will get. As we can see from the illustration, the response is strongly dependent on the eigenfrequency of the vessel. This is because of the response variable is squared in the response spectrum equation shown in Equation 3.33.

In Table 5.9, the standard deviation of the roll motion is presented for each sea state with Hs = 4.5m. The variance is the same as the standard deviation squared, and describes the area below the response spectrum given by Equation 3.53. This is also a measure of the amount of energy in the response spectrum.

Table 5.9: Standard deviation

	FD	TD
Tp = 7.5	0.0694	0.0664
Tp = 8.5	0.1033	0.1012
Tp = 9.5	0.1598	0.1610
Tp = 10.5	0.2793	0.3096
Tp = 11.5	0.4652	0.5149
Tp = 12.5	0.6753	0.7156

As presented in the table above, the standard deviation from the TD and FD analysis is pretty similar. If we study the standard deviation for Tp = 9.5s, we can see that they have an almost identical standard deviation. In Figure 5.18a, the response spectrum is illustrated for the same sea state in TD and FD, with a considerable difference in shape of the spectrum. This difference indicates an equal amount of energy in the two spectra, but the distribution of the energy is different in the TD and FD analysis. In the response spectrum obtained in the FD analysis, there is more energy at the lower wave frequencies, and at a wave frequency around 0.6 [rad/s]. While the energy in the response spectrum obtained from the TD analysis has more energy around the wave peak-frequency. This could be due to the difference in coupling effects from the TD and FD analysis.

5.4 Source of error

In this section, potential reasons for the difference in results computed in TD and FD will be discussed. From Equation 3.33, the equation for the response spectrum $S(\omega)$, we can see that the response spectrum depends on the motion RAO squared, and the wave spectrum. Hence, we can investigate each term to see where the majority of the error has its origin. In Figure 5.21, the JONSWAP spectrum with peak period Tp equal to 11.5 is presented.

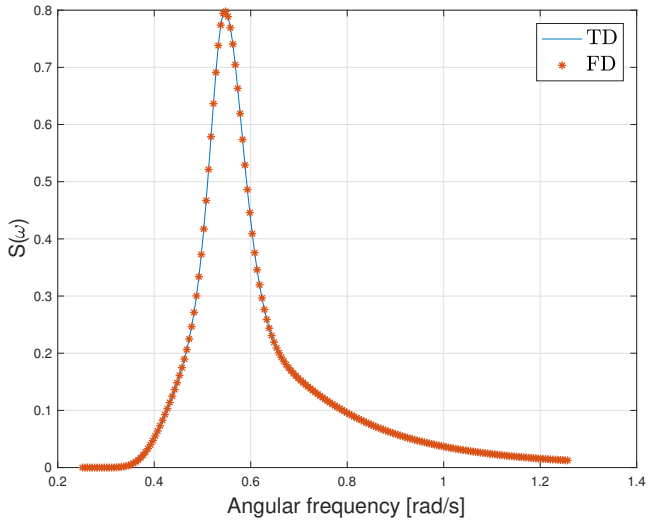

Figure 5.21: JONSWAP Hs = 1.5m, Tp = 11.5s

Based on this figure, we can exclude the wave spectrum as a source for error, since they are identical for the TD and FD analysis.

From this we may say that the error is due to some differences in the motion response. However, it can be many reasons for the error in the response. First of all, it can be due to some differences in the model, parts of the model is imported to SIMA from WADAM, but some restoring values had to be included to prevent the barge from drifting. When restoring is added to yaw and sway, we will get eigenfrequencies in this two DoF. If the eigenfrequencies are close to the eigenfrequency in roll motion they may contribute to motion in roll, since they are coupled.

Another source could be the way damping is included into the two software. In WADAM there is two ways to give additional linear damping as an input. The first one is the linear damping term B_1[Nms], the second way is by including linear damping as a fraction of critical damping given by equation 3.55 and 3.56. The response is very sensitive around the eigenfrequency, hence the number of decimals has a significant impact on the results. An illustration of the difference in response when using B_1, compared to linear damping as a fraction of critical damping is shown in Figure 5.22.

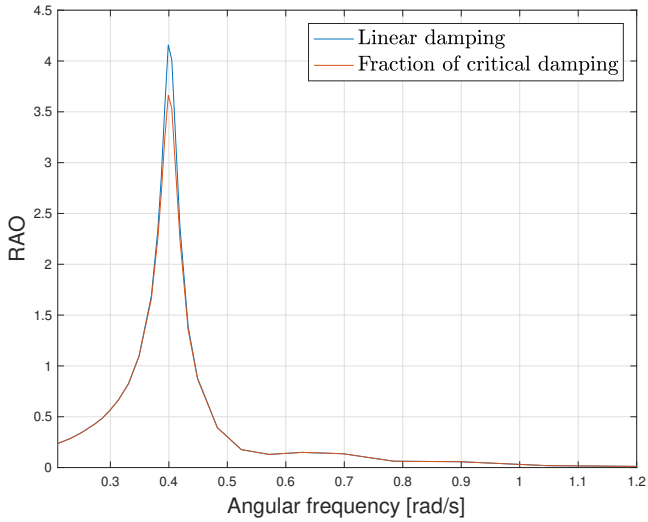

Figure 5.22: Comparison of linear damping and fraction of critical damping

The difference in RAO is about 0.5, which is a significant difference. Using fraction of critical damping as an input, the damping will be larger than for the linear damping B_1 as input.

Chapter 6

Conclusion and recommendations for further work

6.1 Conclusion

The main purpose of this thesis was to do a stochastic linearization of the quadratic roll damping for various sea states, to be able to do a frequency domain analysis of the roll motion. To verify the results, they were compared with the time domain results from a parallel thesis work. This process has formed the basis for analyses of fatigue damage from inertia loads due to wave-induced motions of the vessel.

The biggest challenge of this thesis was to get the model in the time domain analysis to be comparable to the time domain model. It was very time-consuming to solve the problem, but the final models was in the end comparable.

Two analyses cases were done, one with regular waves to compare the model, and one with irregular waves to implement the stochastic linearization method. A wave direction of 45, and 90 degrees was considered for both cases. For the irregular wave case it was several sea states tested, and the resulting response spectrum was compared with the results obtained in the time domain analysis.

The final results coincided very well, and can be used for further work.

6.2 Recommendations for further work

- To be able to use the data obtained in this project to something more useful, the results from the TD and FD should preferably be more equal than the results obtained in this analysis.
- In this analysis we considered a few sea states. To get a more comprehensive picture of how the quadratic damping is affected by the sea sate, we need to check for more sea states. Best way to do it is to consider a sailing rout, and find the most probable sea states.
- If we compute the acceleration from the wave spectra, we can do a global fatigue analysis of the jacket.
- Furthermore, we can look closer at the jacket, and do a local analysis the jacket. By doing this we can see which elements that are vulnerable, and should be considered reinforced to increase the lifetime of the jacket.

Bibliography

Bøe, T., Yang, L., & Falkenberg, E. 2017. The consequence method - An approach for estimating roll damping in transportation fatigue analyses. *In: OMAE 2017.*

Chakrabarti, Subrata. 2000. Empirical calculation of roll damping for ships and barges.

Chakrabarti, Subrata H. 2005. *Handbook of Offshore Engineering.* Elsevier Ltd.

Cozijn, Hans, Uittenbogaard, Ries, & ter Brake, Erik. 2005. Heave, Roll and Pitch Damping of a Deepwater CALM Buoy with a Skirt. *In: International Offshore and Polar Engineering conference.*

DNV-RP-H103. 2011. *DNV-RP-H103 Recommended Practice Modelling and Analysis of Marine Operations.* Det Norske Veritas AS.

DNV-Software. 2005. WADAM - Sesam User Manual.

DNV-Software. 2008. HydroD - Sesam User Manual.

DNV-Software. 2014. Sesam Genie brochure.

DNVGL-Software. 2016. Postresp - Sesam User Manual.

DNVGL-Software. 2017. WADAM - Sesam User Manual.

DNVGL-ST-N001. 2016. DNVGL-ST-N001.

Faltinsen, O. M. 1990. *Sea loads on ships and offshore structures.* Cambridge University Press 1990.

Falzarano, J., Somayajula, A., & Seah, R. 2015. An overview of the prediction methods for roll damping of ships. *Techno-Press*.

Greco, Marilena. 2012. *TMR 4215 Sea Loads Lecture notes*.

Hasselmann, H., Barnett, T.P., Bouws, E., Carlson, H., Cartwright, D.E., Enke, K., Ewing, J.A., Gienapp, H., Hasselmann, D.E., Kruseman, P., Meerburg, A., Muller, P., Olbers, D.J, Richter, K., Sell, W., & Walden, H. 1973. Measurements of Wind-Wave Growth and Swell Decay during the Joint North Sea Wave Project (JONSWAP).

Hemeno, Yoji. 1981. *Prediction of Ship Roll Damping - Sate of the Art*. Tech. rept. University of Osaka Prefecture.

Ikeda, Yoshiho, Hemeno, Yoji, & Tanaka, Norio. 1978. *A Prediction Method for Ship Roll Damping*. Tech. rept. University of Osaka Prefecture.

Journée, J.M.J, & Massie, W.W. 2001. *Offshore Hydromechanics*. Delft University of Technology.

Kato, H. 1966. Effect of Bilge Keels on the Rolling of Ships.

Langen, Ivar, & Sigbjornsson, Ragnar. 1979. *Dynamisk analyse av konstruksjoner (In norwegian, it is translated in a compendium in TMR4305*. Tapir.

Larsen, Carl M. 2012. *TMR 4182 Marine dynamics*.

Myrhaug, Dag. 2004. *Marine dynamics - Stochastic Analysis of Marine Structures - TMR4180*. NTNU-trykk.

Natskår, Asle, & Moan, Torgeir. 2010. Experimental Investigation of Barge Roll in Severe Beam Seas. *COPPE*.

Natskår, Asle, & Steen, Sverre. 2013. Rolling of a transport barge in irregular seas, a comparison of motion analyses and model tests. *CeSOS*.

Ochi, Michel K. 1990. *Applied Probability and Stochastic Processes In Engineering and Physical Sciences*. John Wiley and Sons.

Pettersen, Bjørnar. 2007. *Marin teknikk 3 Hydrodynamikk (In Norwegian)*. NTNU-trykk.

Tanaka, N. 1960. A Study on the Bilge Keel, Part 4. On the Eddy-Making Resistance to the Rolling of a Ship Hull.

Yang, L., Bøe, T., Falkenberg, E., & Korbijn, F. 2018. Variance of fatigue damage during transportation. *In: OMAE 2018*.

Appendices

6.3 Appendix A: Scatter diagram

Table 4.1 Joint frequency of significant wave height H_{m0} and spectral peak period T_p. Data from Tromsøflaket in the period 1977 – 1981 (from Haver, 1985b).

T_p [s] / H_{m0} [m]	0.0 - 1.5	1.5 - 3.0	3.0 - 4.5	4.5 - 6.0	6.0 - 7.5	7.5 - 9.0	9.0 - 10.5	10.5 - 12.0	12.0 - 13.5	13.5 - 15.0	15.0 - 16.5	16.5 - 18.0	18.0 - 19.5	19.5 - 21.0	21.0 - 22.5	22.5 - 24.0	24.0 - 25.5	SUM	KUMULATIV SUM
0.0-0.5	2	1	6	13	2	1	8	5	3	1								42	42
0.5-1.0	2	7	101	238	418	157	74	75	43	6	8	5	1	1				1136	1178
1.0-1.5			54	441	780	450	175	119	79	38	16	10	2	3		1		2168	3346
1.5-2.0			7	254	662	593	258	121	94	66	50	22	9	1				2137	5483
2.0-2.5				72	512	613	324	130	78	42	37	16	9	1				1834	7317
2.5-3.0				11	264	498	299	140	79	34	23	14	1	1				1364	8681
3.0-3.5				3	85	349	253	121	63	30	12	8						924	9605
3.5-4.0					24	188	218	119	59	18	9	5						640	10245
4.0-4.5					4	85	135	94	54	17	12	2						403	10648
4.5-5.0						28	102	87	57	18	2			1				295	10943
5.0-5.5						11	51	82	38	10	4	2						198	11141
5.5-6.0						1	15	48	31	10	1		1					107	11248
6.0-6.5							8	32	22	5	1							68	11316
6.5-7.0							4	15	19	10	5							53	11369
7.0-7.5							2	4	16	7	1	1						31	11400
7.5-8.0							1	2	7	5	2						1	18	11418
8.0-8.5							2		7	5		1						15	11433
8.5-9.0									2	2	3							7	11440
9.0-9.5									1	8	1							10	11450
9.5-10.0										1	1							2	11452
10.0-10.5																			11452
10.5-11.0												1						1	11453
11.0-11.5											1							1	11454
11.5-12.0																			11454
12.0-12.5												1						1	11455
SUM	4	8	168	103	2751	2974	1929	1194	752	333	189	88	23	8		1	1	11455	

Figure 6.1: Scatter diagram from Tromsøflaket

6.4 Appendix B: Response spectra from irregular waves

Hs = 1.5 m

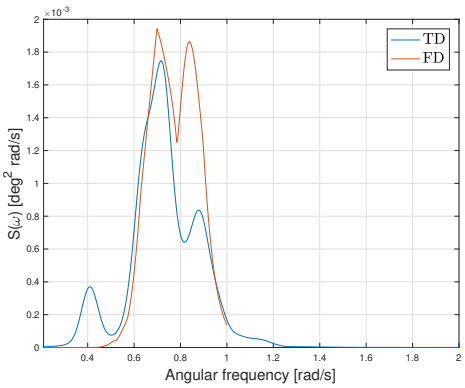

(a) Tp=7.5s, 45deg

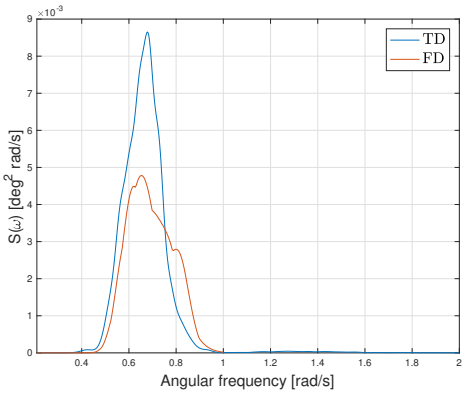

(b) Tp=7.5s, 90deg

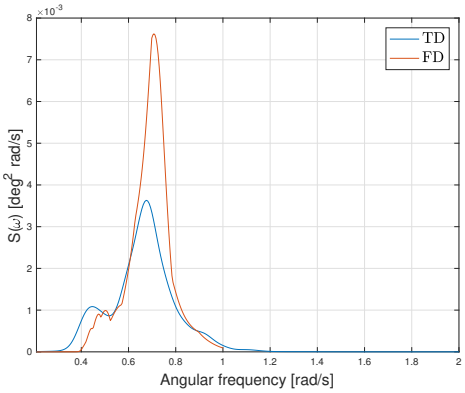

(c) Tp=8.5s, 45deg

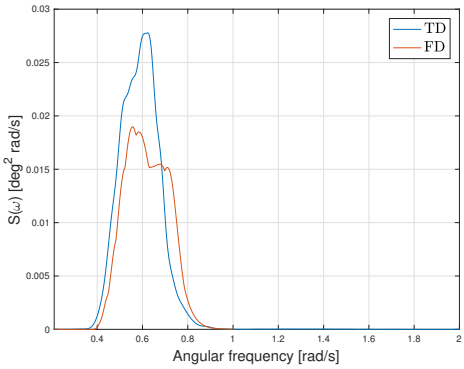

(d) Tp=8.5s, 90deg

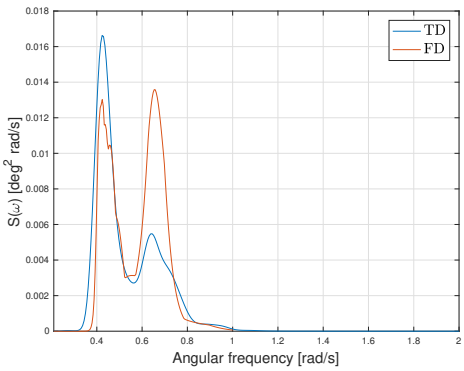

(e) Tp=9.5s, 45deg

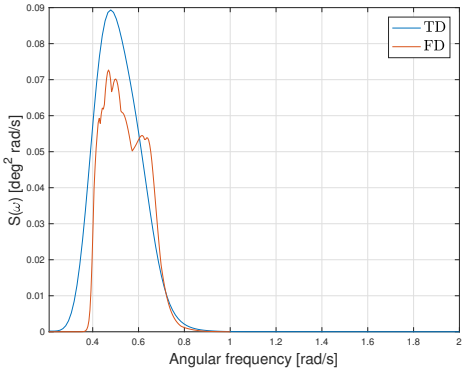

(f) Tp=9.5s, 90deg

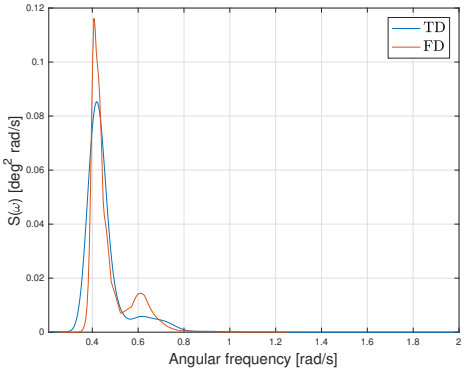

(g) Tp=10.5s, 45deg

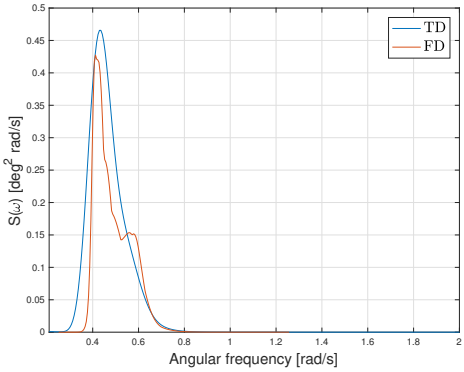

(h) Tp=10.5s, 90deg

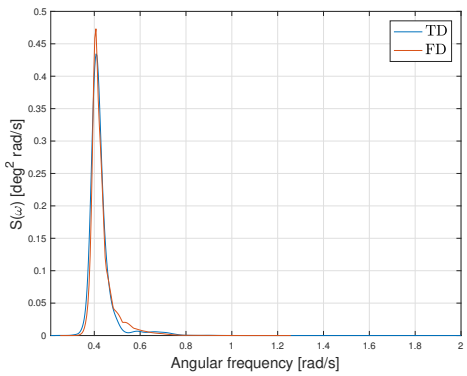

(i) Tp=11.5s, 45deg

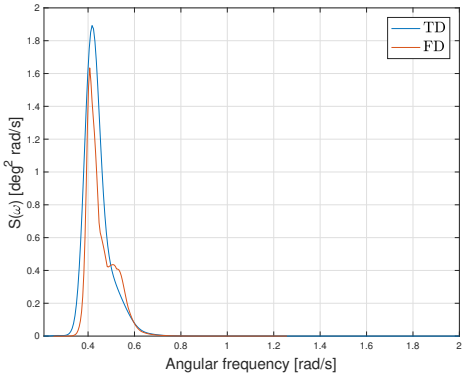

(j) Tp=11.5s, 90deg

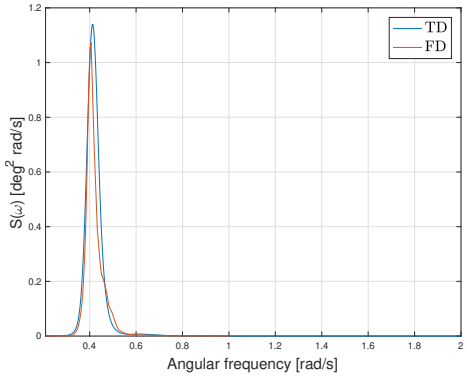

(k) Tp=12.5s, 45deg

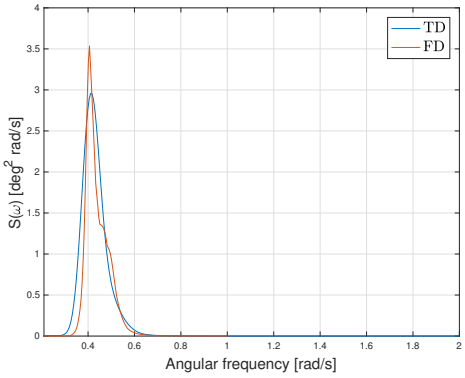

(l) Tp=12.5s, 90deg

Figure 6.2: Response spectrum for Hs = 1.5m

Hs = 2.5 m

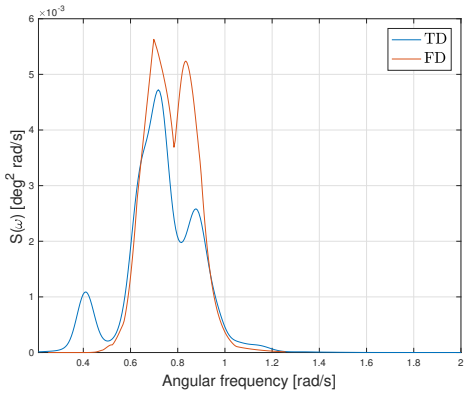

(a) Tp=7.5s, 45deg

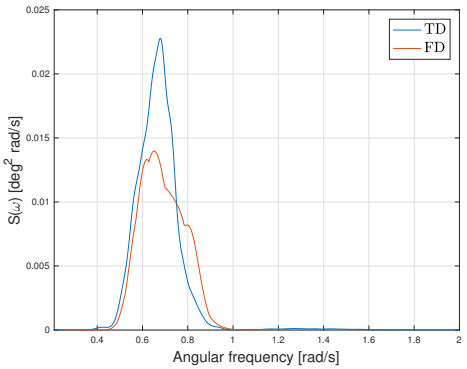

(b) Tp=7.5s, 90deg

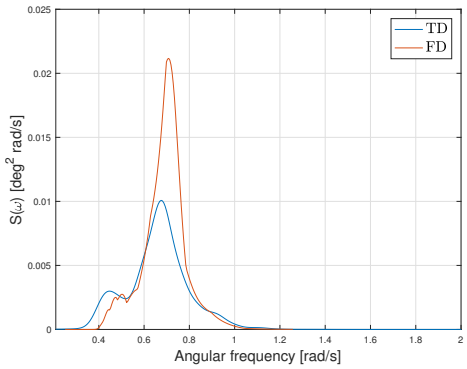

(c) Tp=8.5s, 45deg

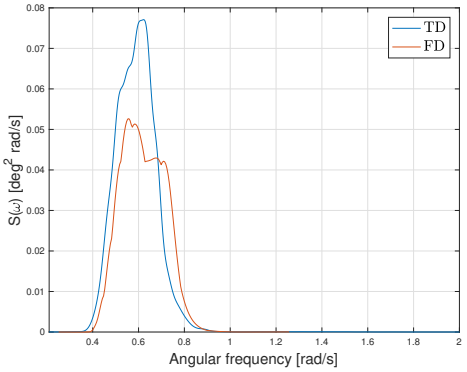

(d) Tp=8.5s, 90deg

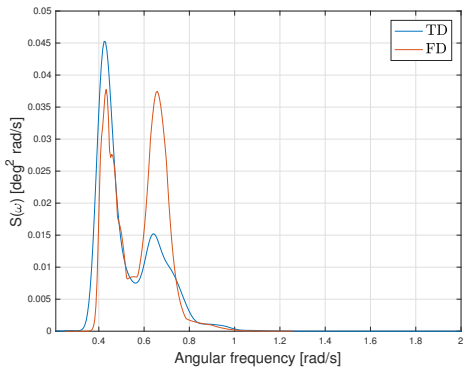

(e) Tp=9.5s, 45deg

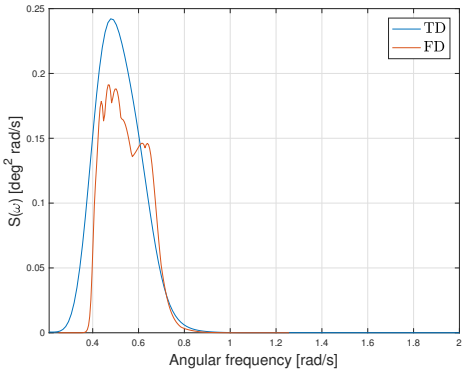

(f) Tp=9.5s, 90deg

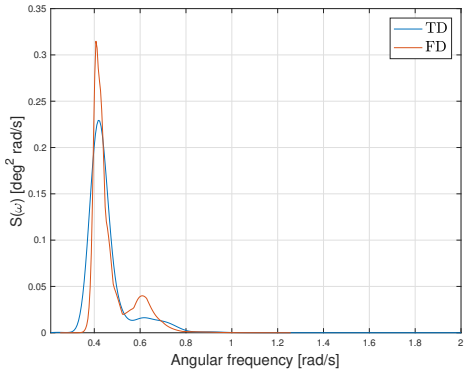

(g) Tp=10.5s, 45deg

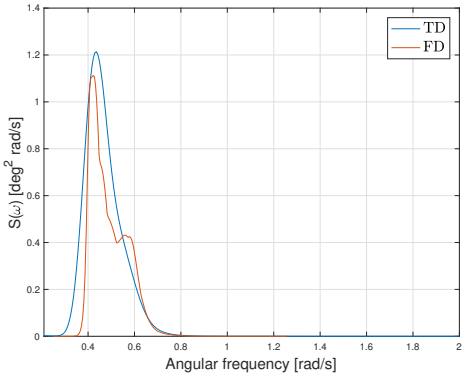

(h) Tp=10.5s, 90deg

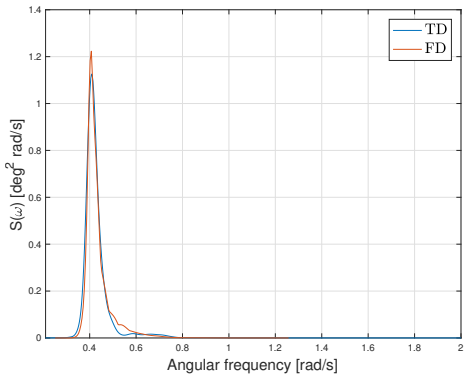

(i) Tp=11.5s, 45deg

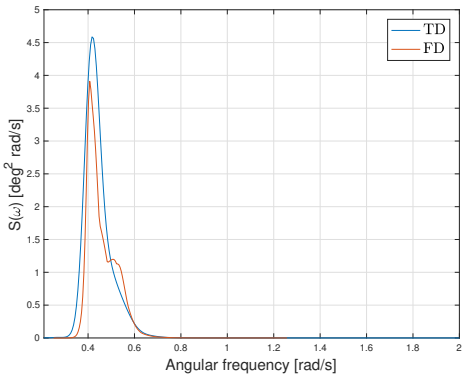

(j) Tp=11.5s, 90deg

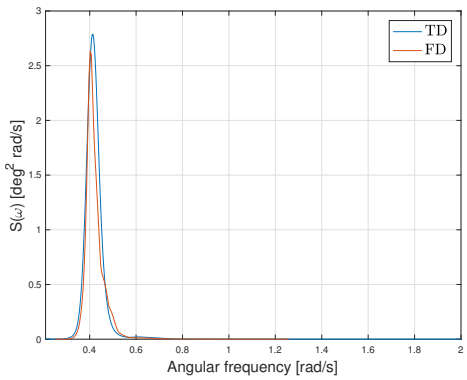

(k) Tp=12.5s, 45deg

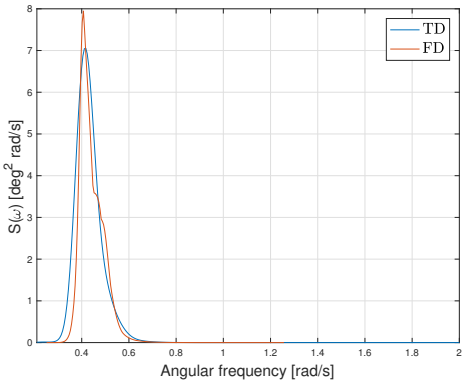

(l) Tp=12.5s, 90deg

Figure 6.3: Response spectrum for Hs = 2.5m

Hs = 3.5 m

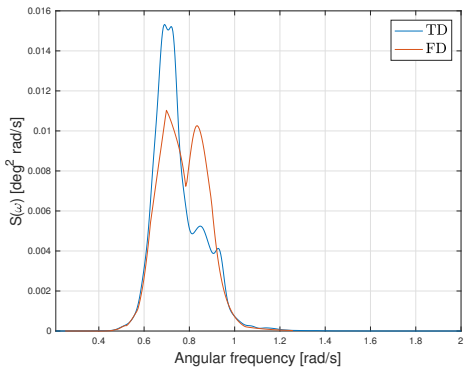

(a) Tp=7.5s, 45deg

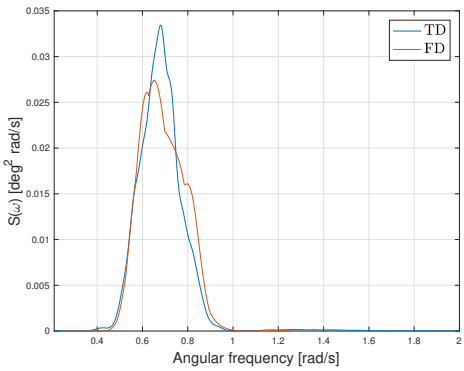

(b) Tp=7.5s, 90deg

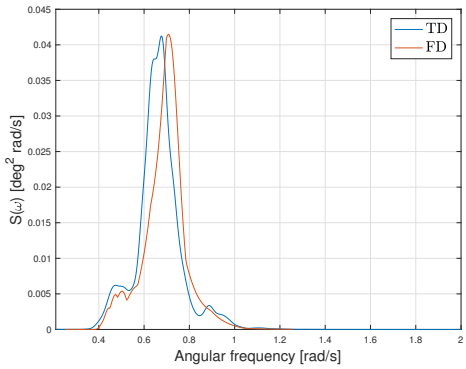

(c) Tp=8.5s, 45deg

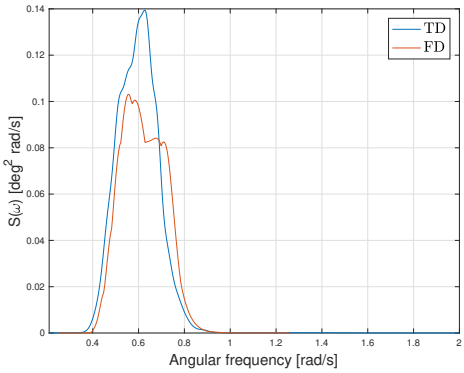

(d) Tp=8.5s, 90deg

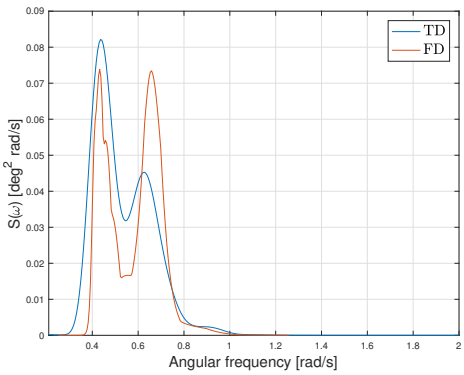

(e) Tp=9.5s, 45deg

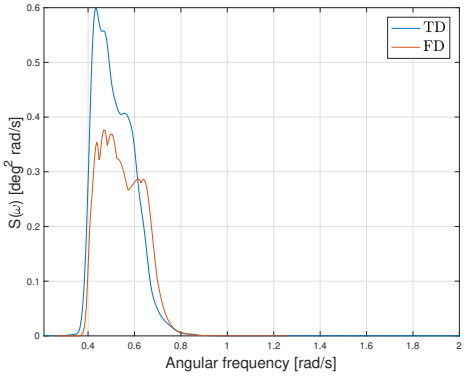

(f) Tp=9.5s, 90deg

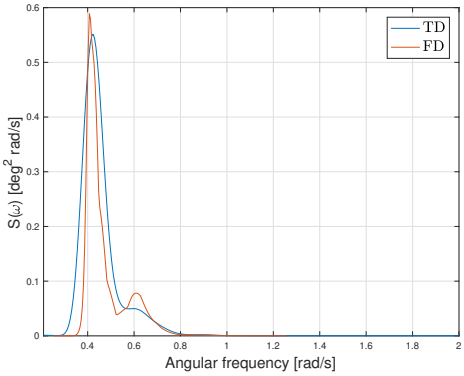

(g) Tp=10.5s, 45deg

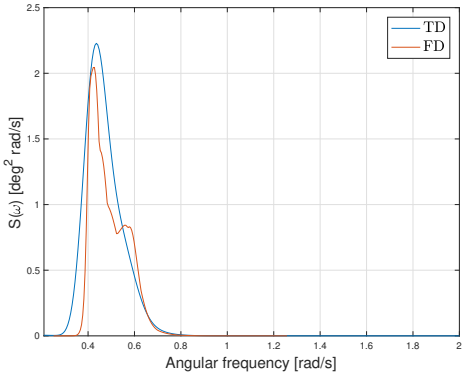

(h) Tp=10.5s, 90deg

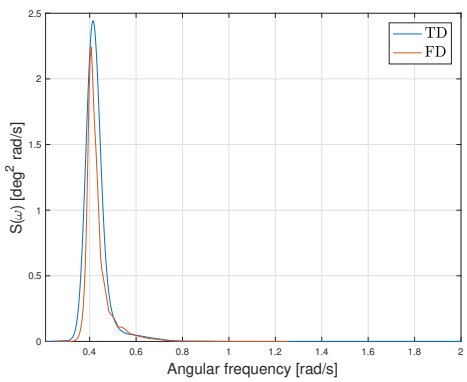

(i) Tp=11.5s, 45deg

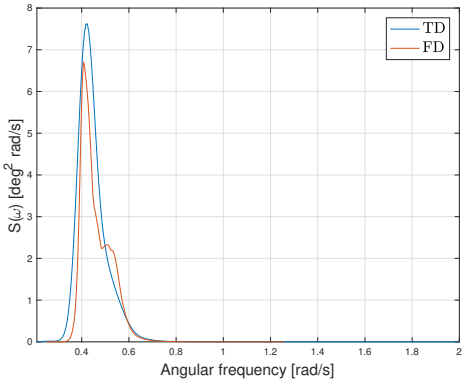

(j) Tp=11.5s, 90deg

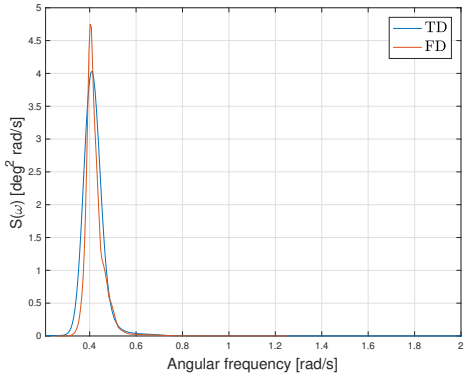

(k) Tp=12.5s, 45deg

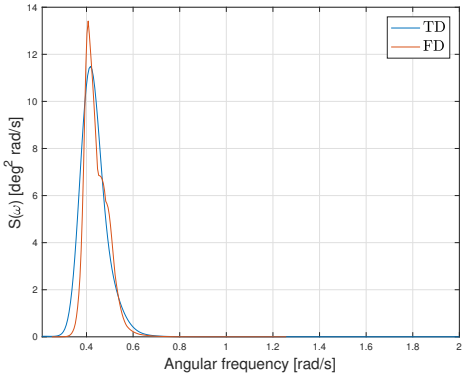

(l) Tp=12.5s, 90deg

Figure 6.4: Response spectrum for Hs = 3.5m

Hs = 4.5 m

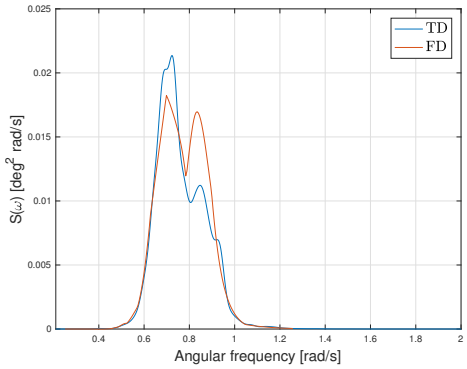

(a) Tp=7.5s, 45deg

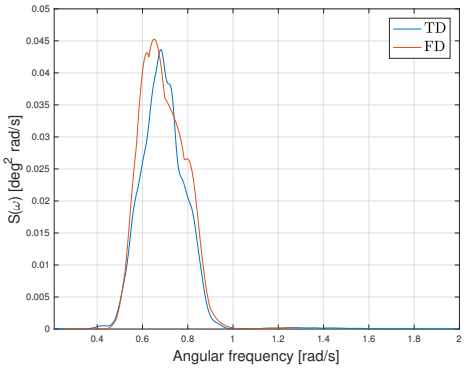

(b) Tp=7.5s, 90deg

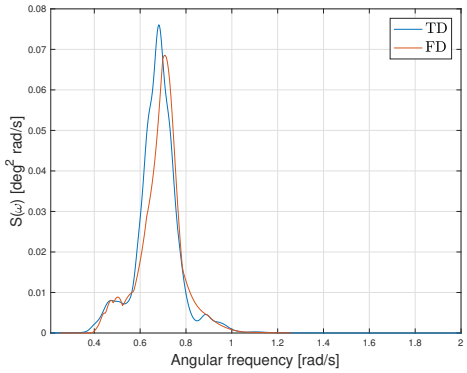

(c) Tp=8.5s, 45deg

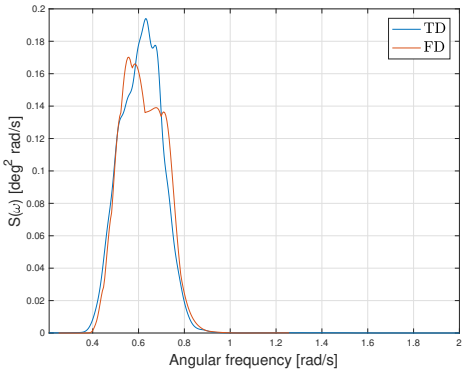

(d) Tp=8.5s, 90deg

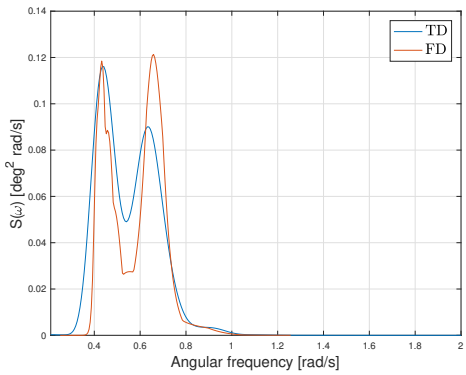

(e) Tp=9.5s, 45deg

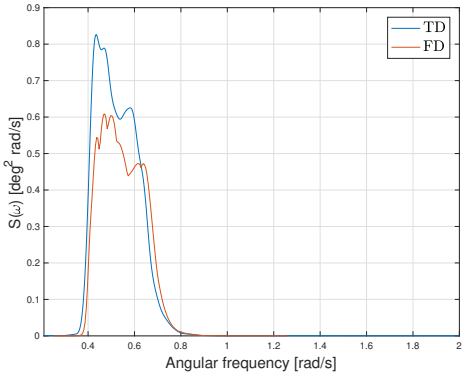

(f) Tp=9.5s, 90deg

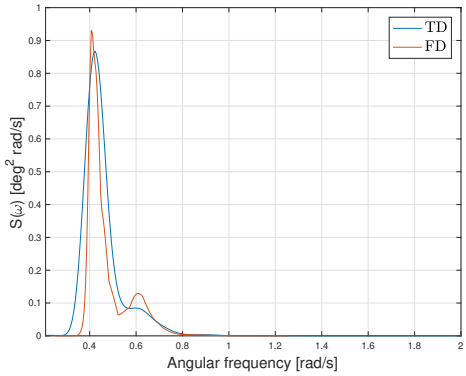

(g) Tp=10.5s, 45deg

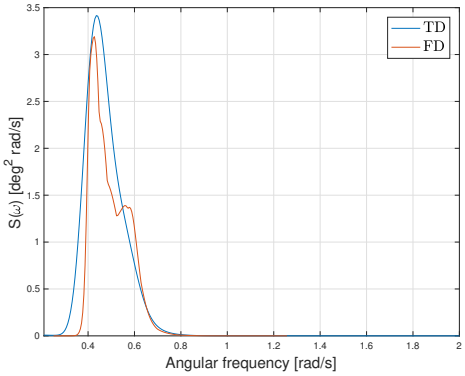

(h) Tp=10.5s, 90deg

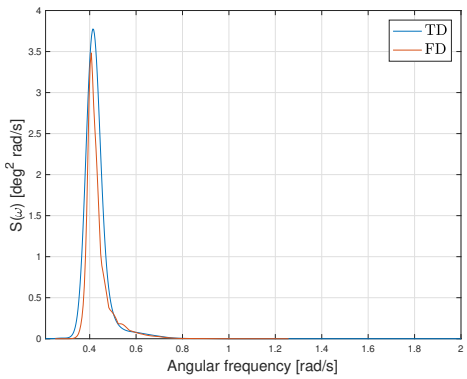

(i) Tp=11.5s, 45deg

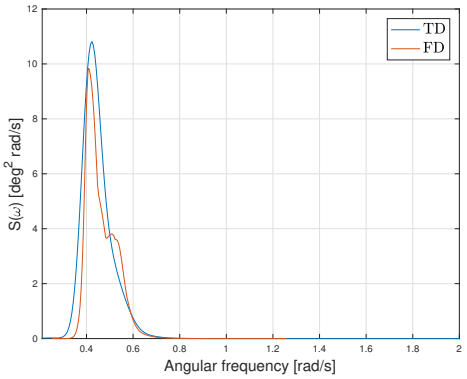

(j) Tp=11.5s, 90deg

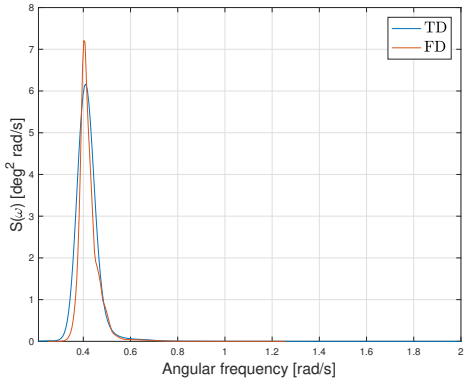

(k) Tp=12.5s, 45deg

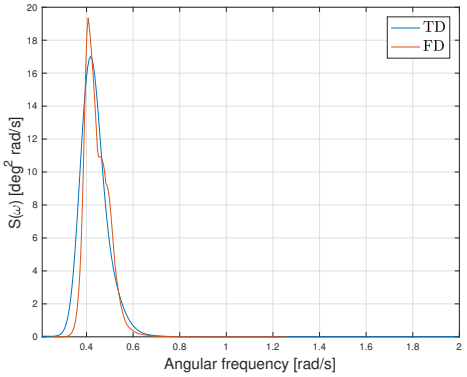

(l) Tp=12.5s, 90deg

Figure 6.5: Response spectrum for Hs = 4.5m

Hs = 5.5 m

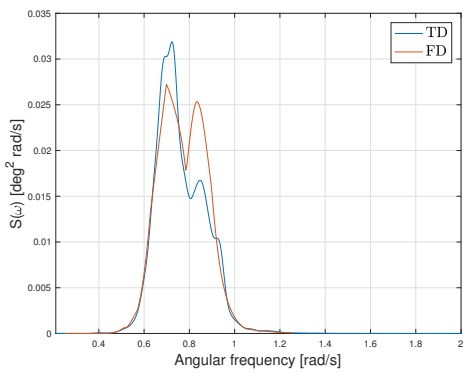

(a) Tp=7.5s, 45deg

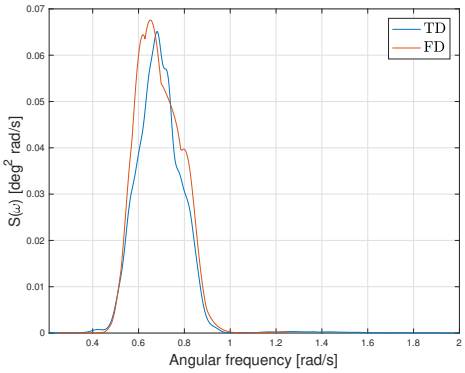

(b) Tp=7.5s, 90deg

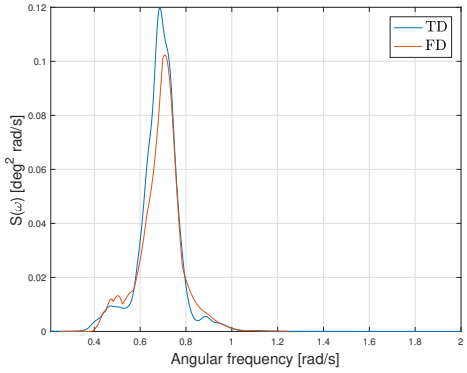

(c) Tp=8.5s, 45deg

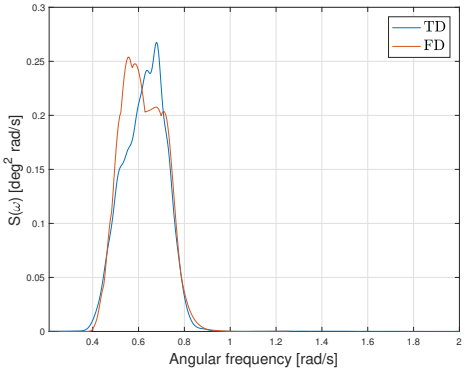

(d) Tp=8.5s, 90deg

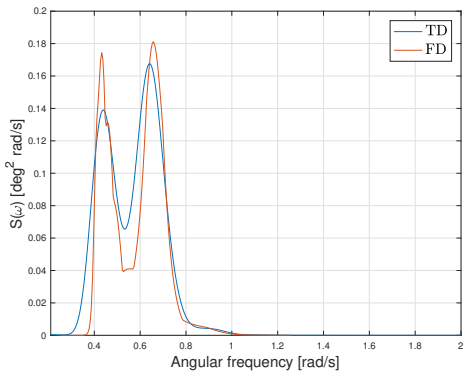

(e) Tp=9.5s, 45deg

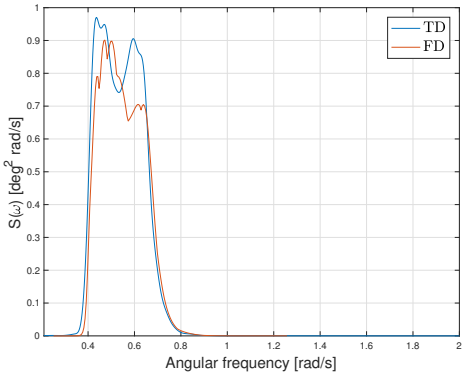

(f) Tp=9.5s, 90deg

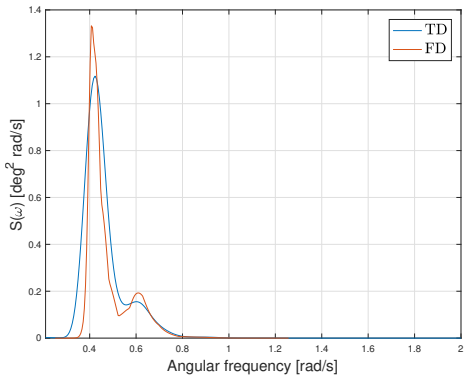

(g) Tp=10.5s, 45deg

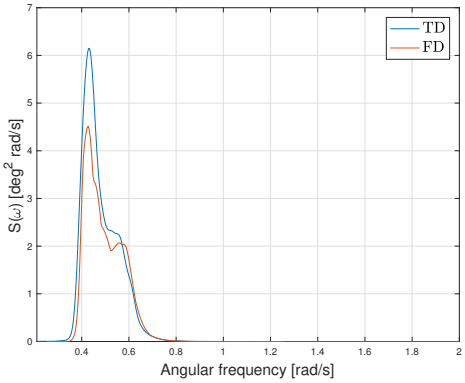

(h) Tp=10.5s, 90deg

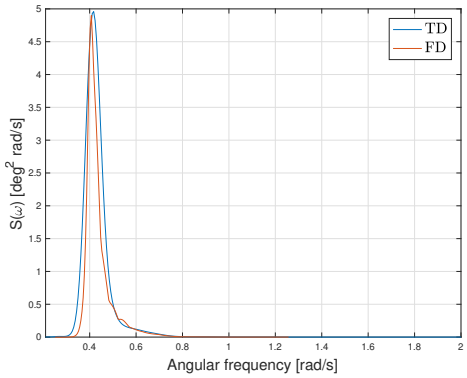

(i) Tp=11.5s, 45deg

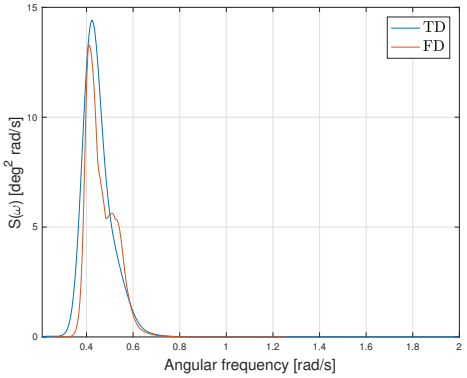

(j) Tp=11.5s, 90deg

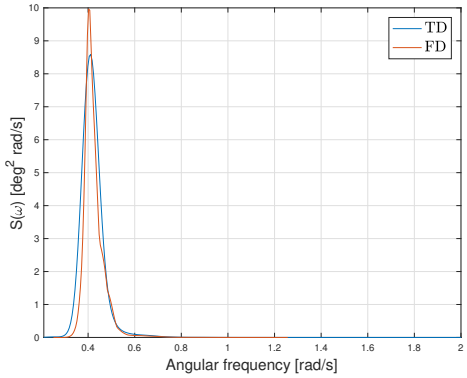

(k) Tp=12.5s, 45deg

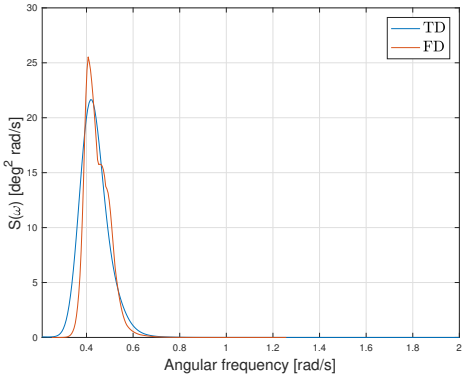

(l) Tp=12.5s, 90deg

Figure 6.6: Response spectrum for Hs = 5.5m

Hs = 6.5 m

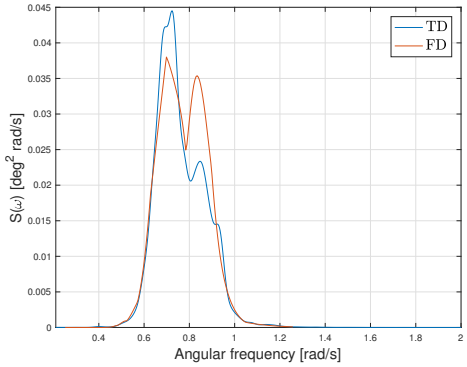

(a) Tp=7.5s, 45deg

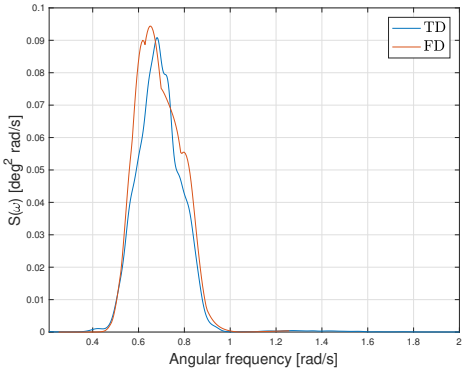

(b) Tp=7.5s, 90deg

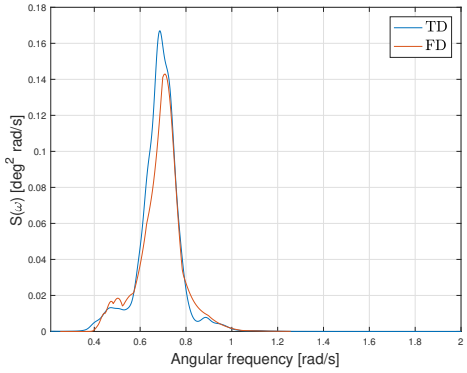

(c) Tp=8.5s, 45deg

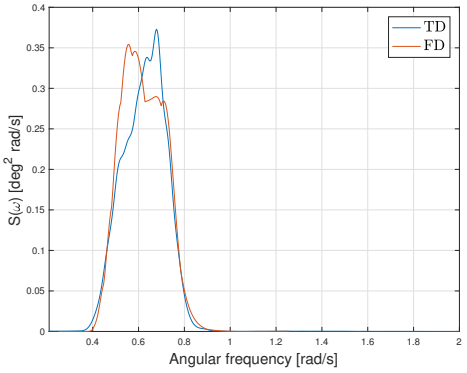

(d) Tp=8.5s, 90deg

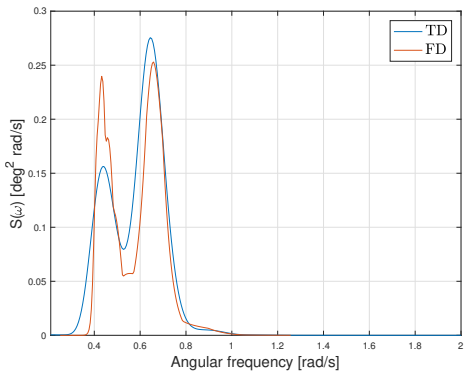

(e) Tp=9.5s, 45deg

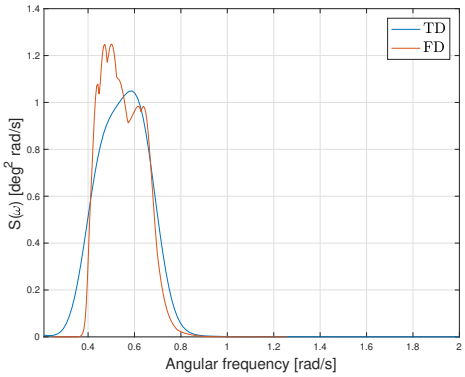

(f) Tp=9.5s, 90deg

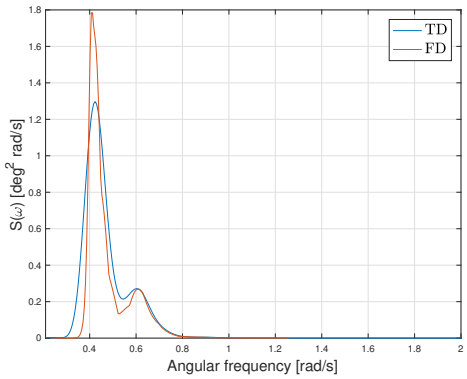

(g) Tp=10.5s, 45deg

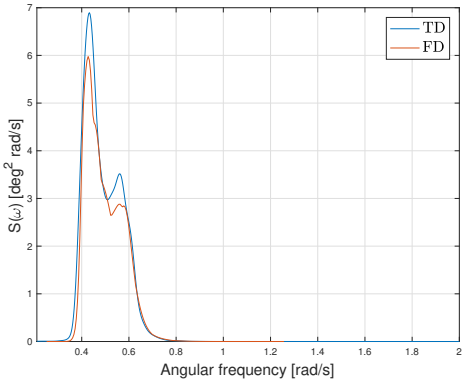

(h) Tp=10.5s, 90deg

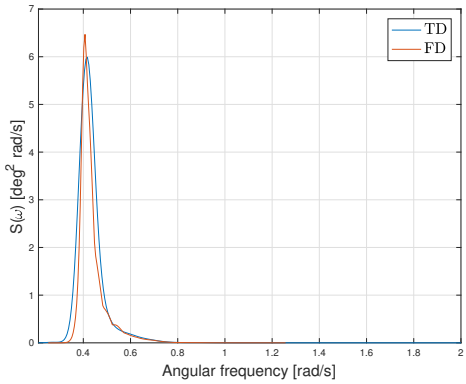

(i) Tp=11.5s, 45deg

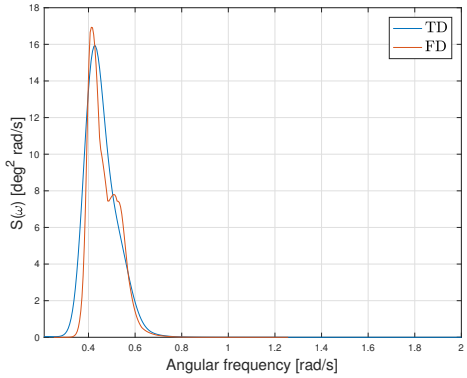

(j) Tp=11.5s, 90deg

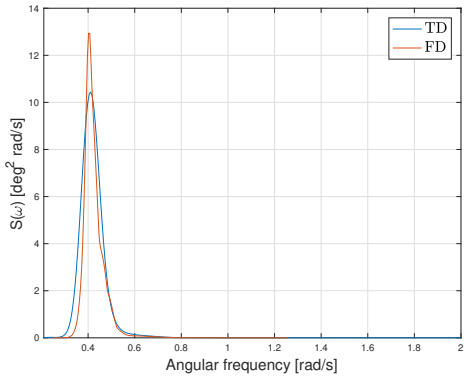

(k) Tp=12.5s, 45deg

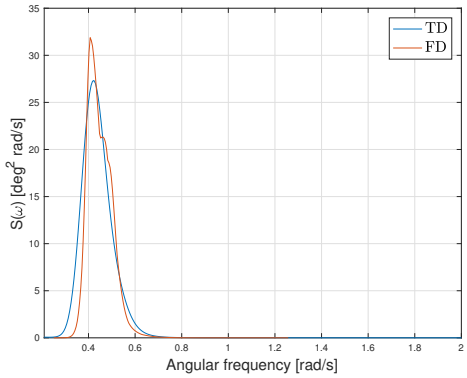

(l) Tp=12.5s, 90deg

Figure 6.7: Response spectrum for Hs = 6.5m